Results in Optics 9 (2022) 100285

Contents lists available at ScienceDirect

Results in Optics

journal homepage: www.sciencedirect.com/journal/results-in-optics

Integrated optical bimodal waveguide biosensors: Principles and applications

Luis Torrijos-Morán [a,c,*], Bárbara D. Lisboa [b], Maria Soler [b], Laura M. Lechuga [b], Jaime García-Rupérez [a,*]

[a] Nanophotonics Technology Center, Universitat Politècnica de València, 46022 Valencia, Spain
[b] Nanobiosensors and Bioanalytical Applications Group (NanoB2A), Catalan Institute of Nanoscience and Nanotechnology (ICN2), CSIC, BIST and CIBER-BBN, 08193 Bellaterra, Barcelona, Spain
[c] Currently at Photonics Research Labs, iTEAM Research Institute, Universitat Politècnica de València, 46022 Valencia, Spain

ARTICLE INFO

Keywords:
Optical biosensors
Integrated optics
Bimodal waveguides
POC devices
LOC systems

ABSTRACT

Integrated optical biosensors have become one of the most compelling technologies for the achievement of highly sensitive, multianalyte, portable and easy to use point-of-care (POC) devices with tremendous impact in healthcare and environmental protection, among other application fields. In this context, bimodal waveguide (BiMW) interferometers have emerged over the last years as a powerful biosensor technology providing the benefits of extreme sensitivity under a label-free scheme, reliability and robustness within a highly compact footprint that can be integrated and multiplexed in lab-on-a-chip (LOC) platforms. In this review, we provide an overview of the state-of-the-art about integrated optical BiMW biosensors from the theoretical fundamentals to their practical implementation. Furthermore, we explore recent advances such as novel designs, integration in specific LOC systems and its application in real biosensing scenarios. Final remarks and perspectives on the potential impact of these biosensor interferometric structures are also provided, as well as some limitations that must be addressed in next steps.

1. Introduction

Optical biosensors are devices able to detect a certain amount of a specific analyte by means of its interaction with an optical signal (McDonagh et al., 2008; Ligler, 2009). They provide several advantages in terms of selectivity, sensitivity and real-time response, which ultimately allows performing the detection without the need of target labelling or amplification steps. These advantages make photonic biosensors suitable for point-of-care (POC) applications such as early diagnosis of diseases, environmental monitoring, or food quality control, among others (González-Guerrero et al., 2016). Moreover, they can be easily integrated in very small chips compatible with complementary metal-oxidesemiconductor (CMOS) technology, which enables multiplexed detection and low-cost mass production. To this end, the miniaturization of photonic biosensors that can be portable in lab-on-a-chip (LOC) platforms is of great interest. These schemes include all kind of functionalities needed to perform an analysis, from microfluidics to read-out systems, in order to provide results that can be easily interpreted by nonskilled personnel (Estevez et al., 2012; Duval et al., 2012).

Within this field, integrated optics (IO) play a prominent role in the development of LOC devices as they offer high potential for chip miniaturization within tiny areas. They consist of compact light guiding structures capable of detecting the substance of interest via evanescent wave mechanism (Lambeck, 1992; Lambeck, 2006), where part of the electromagnetic field is spread out outside the waveguide core, thus interacting with the surrounding volume. The most employed evanescent field sensors over the years have been plasmonic ones due to their simplicity and ability for detecting biological targets (Soler et al., 2019; Lopez et al., 2017). However, in some cases, plasmonic label-free sensitivities are not high enough for real clinical and environmental applications, which can be at the pM-nM level for common biomarkers, but in the range of aM-fM concentrations for novel biomarkers or trace elements. Also, the integration of plasmonic biosensors in LOC systems is more complex than for IO sensors, especially due to the need of bulky light coupling schemes (e.g., Kretschmann configuration), limited CMOS compatibility of plasmonic metals like gold, or the sophisticated nanofabrication methods required for nanoplasmonic sensor design. In contrast, silicon-based integrated sensors provide extremely high

* Corresponding authors.
E-mail addresses: luistm@upv.es (L. Torrijos-Morán), jaigarru@upv.es, arru@ntc.upv.es (J. García-Rupérez).

https://doi.org/10.1016/j.rio.2022.100285
Received 4 May 2022; Received in revised form 17 July 2022; Accepted 28 July 2022
Available online 1 August 2022

sensitivities (up to pM-fM level) in compact devices that can be easily miniaturized and multiplexed (Fernández Gavela et al., 2016; Luan et al., 2018). Different types of silicon-based optical sensors can be found in the literature depending on its configuration and waveguide structure. The most relevant examples are interferometers, grating couplers, ring resonators (RR), photonic crystals (PC), silicon wire, slot-waveguide based systems and subwavelength gratings (SWG). Although they all operate via evanescent-wave mechanism, their different waveguide structure provides different quantifiable properties and performance such as the bulk and surface sensitivity or the detection limit. For instance, RR and PC structures have shown great potential due to their highly compact footprint and high throughput analysis (Ksendzov and Lin, 2005; Chow et al., 2004; Chrostowski et al., 2012). Besides, these sensors can be improved by combining them with slot-waveguides or SWG, thus increasing the waveguide sensitivity (Cheben et al., 2018; Wangüemert-Pérez et al., 2019; Barrios et al., 2008). Nonetheless, interferometric configurations are probably the most attractive for biosensing as they provide higher sensitivity values and lower detection limits, typically around 10^{-8} RIU, more than one order of magnitude better than the aforementioned schemes. Among other configurations, Mach-Zehnder (MZI) and Young (YI) interferometers are the most used for biosensing purposes (Heideman and Lambeck, 1999; Ymeti et al., 2003). In an interferometric configuration, light is split into two different optical paths or arms and recombined afterwards in the case of the MZI. A general approach is to design one of the arms isolated as a reference and the other interacting with the substance of interest. Since the evanescent field of the guided light slightly extends into the surrounding medium, any change of the refractive index (RI) of the medium will directly affect the light phase of the sensing arm, causing a phase difference between the paths at the recombined output. In this way, the binding of target molecules to the sensor surface will cause a variation of the RI directly proportional to the analyte concentration, which can be monitored and quantified through the phase shift interrogation. Planar MZI schemes were first demonstrated as an immunosensor in the early 1990s (Heideman et al., 1991) and some years later they were fully integrated in a silicon platform (Schipper et al., 1997). Since then, the high number of publications with diverse MZI configurations indicate the impact within the field of integrated optical biosensors (Sepúlveda et al., 2006; Gao et al., 2011; Liu et al., 2013).

Over the last years, another paradigm of interferometric scheme using bimodal waveguides (BiMW) were first introduced theoretically in Levy and Ruschin (2009), where a single-channel waveguide structure supporting two orthogonal modes of the same polarization and with their own propagation constants is designed. By properly placing a single-mode waveguide at the output, the power of both propagating modes is transferred to the fundamental one at that output waveguide, leading to an interferometric response dependent on the differential phase shift between those two modes, as it happens for other interferometric configurations. Later, this approach was experimentally demonstrated in (Zinoviev et al., 2011), where instead of placing an output single-mode waveguide to combine both modes, a photodetector array was placed at the output to measure the free-space interference pattern produced between them, similarly to what happens for Young interferometers. Since the evanescent field of both modes does not equally interact with the sample, a phase shift is produced at the output, as in the case of an MZI. However, in order to achieve low limits of detection, both modes must be equally excited by a single-mode waveguide, which is aligned out-of-axis respect to the bimodal waveguide. This is a non-trivial process and a proper design of the interface between the bimodal and the single-mode part must be addressed to overcome possible limitations in the overall performance. POC devices can benefit from BiMW as they present more compact designs than MZIs (the footprint is reduced at least by a factor two due to the single-channel configuration of the former), which is desirable for the integration of multiple biosensors in a single chip. Additionally, since these BiMW are purely dielectric structures, they can be fabricated using the same processes typically considered for other IO devices, thus preserving CMOS compatibility. Recently, the performance of BiMW has been enhanced by inserting periodic elements in the waveguide design, increasing the optical field interaction within the sensing area, which is translated into a higher sensitivity (García-Rupérez and Torrijos-Morán, 2021; Torrijos-Morán et al., 2020). Two different approaches involving periodic BiMW have been reported depending on whether the wavelength-periodicity ratio operates at the SWG or the PC regime (García-Ruperez et al., 2021). Including periodic configurations provides not only higher light-matter interaction, but also additional dispersive properties in the optical modes, which enhances the sensing features compared to uniform BiMWs.

In this review, we present a comprehensive study of BiMW interferometric biosensors from an analytical to a practical point of view. A description of the fundamentals is provided, focusing on the operation of the evanescent wave principle in this type of structures, and how inserting periodic elements in the BiMW design benefits the sensing response. Later, an overview of the surface functionalization methods and the sensor integration in LOC platforms is reported, as well as recent advances in biosensor experiments for real applications. Finally, in the last part, we discuss the trends, perspectives, and next steps of BiMWs in the near future as one of the most promising IO-based structures for biosensor devices.

2. Fundamentals and design

2.1. Evanescent field sensing principle

With the rapid growth of integrated optics, photonic chips based on thin film technology emerged for all kinds of waveguide-based applications, as in the case of biosensors (Tien, 1977; Soref, 2006). Light propagates through integrated waveguides via total internal reflection due to the high-index-contrast of the materials used. The most employed platform is silicon-on-insulator (SOI) where optical modes are highly confined within the silicon core (Paniccia, 2010). A competitive alternative is silicon nitride, which provides a moderate-index-contrast (around 0.5 compared to 1.5 in the case of SOI) and transparency for visible wavelengths, which is very interesting for biosensing purposes, since most biomolecules (proteins, lipids, and nucleic acids) present structural absorption peaks in the mid-IR region (Muñoz et al., 2017). Common to all these platforms, the effective index is an important parameter that characterizes a certain propagating mode and its surrounding medium. It relates the field distribution of a given mode and polarization with the refractive index of the materials employed in the core and the cladding. It is similar to thinking of a mode propagating straight in an artificial waveguide with an equivalent refractive index n_{eff}.

In a BiMW as the one shown in Fig. 1, two modes of the same polarization and with propagation constants β_1 and β_2, propagate through the same optical waveguide with their own effective indices. As the optical field penetrates in the upper cladding, where the sensing area is located, a variation of the effective indices of the modes is produced (Herranz et al., 2017). This part of the optical signal that interacts with the target analytes is known as evanescent field as it decays exponentially with the distance to the waveguide core (typically 0.1–1 μm). As it is depicted in Fig. 1, the evanescent field is different for each mode in the BiMW, the fundamental mode (β_1) is more confined within the waveguide core than the higher order mode (β_2) which extends throughout the cladding region, resulting in a change of the effective index difference between the modes when the sensing occurs. Interferometric configurations including BiMW biosensors are shown in Fig. 2, which consist of a single-mode waveguide as input and output ports, and a bimodal structure placed in between, where the sensing area is designed. The bimodal part design must be larger than the single-mode waveguides either by increasing its width or height, see Fig. 2b and c

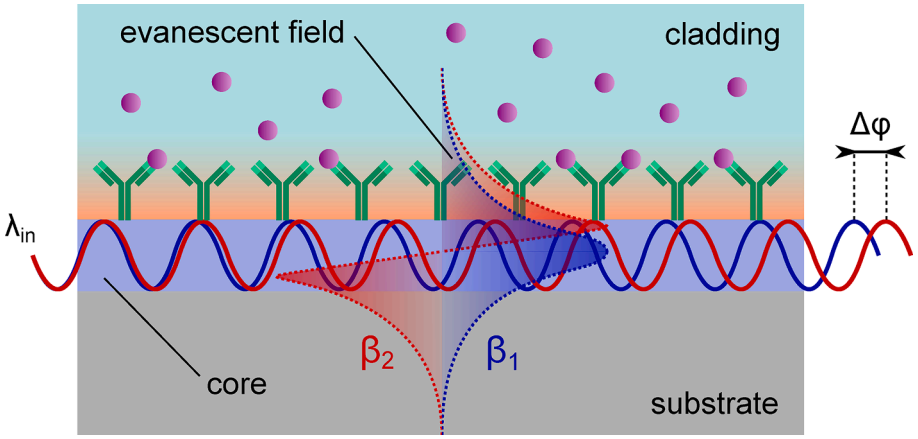

Fig. 1. Scheme of the optical field propagation throughout a BiMW. A typical biosensing scenario in the upper cladding is represented, which is measured via evanescent wave mechanism.

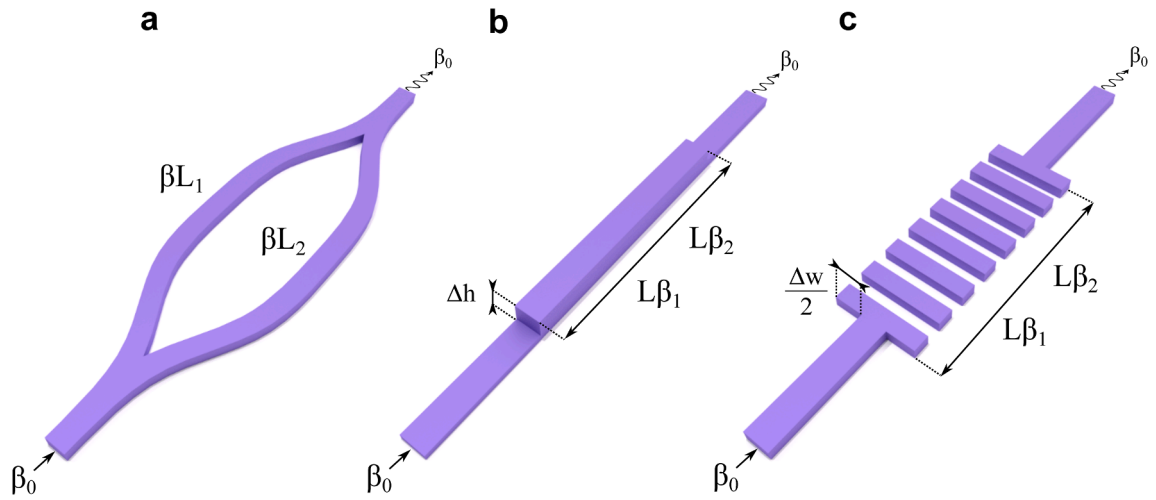

Fig. 2. Schemes of different interferometric sensor types: (a) conventional MZI, (b) uniform bimodal waveguide with increased height and (c) periodic bimodal waveguide with increased width.

respectively, in order to support two electromagnetic modes. In next sections, we explore two different types of BiMW configurations: uniform and periodic in its propagation direction, Fig. 2b and c respectively, and compare both with conventional MZI schemes, Fig. 2a.

2.2. Uniform configurations

Let us start with the simplest configuration: the uniform BiMW shown in Fig. 2b. Internally, it behaves like a MZI: an input optical beam is splitted into two and recombined afterwards to create an interference pattern at the output. In the uniform BiMW case, a single-mode waveguide supporting the fundamental mode of a given polarization excites the first two lower order modes (even and odd parity) of the same polarization in the bimodal region. Similarly, these two modes contribute to the excitation of the fundamental one at the single-mode output waveguide. Due to the wave nature of light, the intensity at the BiMW output can be defined as a sinusoidal function depending on the phase shift accumulated in the bimodal part, as follows

$$I_{out} = I_1 + I_2 + 2\sqrt{I_1 I_2}\cos\Delta\varphi \tag{1}$$

where $I_{1,2}$ are the intensities of the fundamental and higher order modes in the BiMW, respectively, and $\Delta\varphi$ is the phase shift between these two modes for a given wavelength. In turn, the phase shift can be expressed in terms of the effective index as

$$\Delta\varphi = \frac{2\pi}{\lambda}(L_1 n_{eff1} - L_2 n_{eff2}) \tag{2}$$

where λ is the operating wavelength, $L_{1,2}$ are the physical lengths of the optical paths and $n_{eff1,2}$ are the effective indices of the fundamental and higher order modes, respectively. Note that L_1 and L_2 are the same in the BiMW since both modes propagate through the same optical waveguide, whereas $n_{eff1} = n_{eff2}$ in a MZI when the waveguide dimensions of the arms are equally designed. This is the reason why MZI are typically conceived with a large difference between the length of the arms in order to enhance the phase shift accumulated at the output. Likewise, in a BiMW, since both modes propagate through the same optical path, the phase shift is produced as a result of the effective indices difference. Therefore, in a biosensing application, a change in the cladding refractive index produces a variation in the effective index of the propagating modes. Specifically, the sensitivity of a BiMW sensor can be mathematically defined as

$$S = \frac{\Delta\varphi_d}{\Delta n_c} = \frac{2\pi L}{\lambda}\left(\frac{\partial n_{eff2}}{\partial n_c} - \frac{\partial n_{eff1}}{\partial n_c}\right) \tag{3}$$

where $\Delta\varphi_d$ is the phase shift difference when the sensing takes place, and Δn_c is the change of the cladding refractive index. In a conventional MZI

scheme, one of the arms is designed isolated to act as a reference, so that the phase shift will solely depend on the change of the effective index in the sensing arm. In contrast, in a BiMW since both modes interact with the sensing area, they are designed to maximize the effective index difference, specifically to produce a large variation in the higher order mode compared to the fundamental one (typically around a factor of 6). This is because the higher order mode is less confined within the waveguide core and thus more sensitive to cladding refractive index variations than the fundamental one, which in turns acts as reference mode although it is not completely isolated. Note also that both the MZI and BiMW sensitivity directly scales with the device length, which is common to all interferometric-based sensors measuring phase shifts and explains the large footprints typically employed. Because of this fact, the sensitivity is usually normalized to a 1 cm length of the bimodal sensing part so that they can be properly compared.

First modal configurations were introduced as interferometric devices to realize a magneto-optic isolator using a wide strip waveguide etched into two layers (Lohmeyer et al., 2001). Here, the width and thickness of the modal waveguide was studied for optimum performance and fabrication tolerances operating at the near infrared region. Similar modal devices were later presented as temperature sensors by using fully etched silicon waveguides with horizontal modal splitters and optimized dimensions to maximize the sensitivity (Irace et al., 2003). More recently, single-channel structures based on BiMWs were theoretically described for refractive index sensing using vertical symmetry junctions to excite both modes in the sensing area (Gao et al., 2011) and later experimentally demonstrated as biosensors for the first time on a silicon nitride platform, Fig. 3a (Zinoviev et al., 2011). The latter design

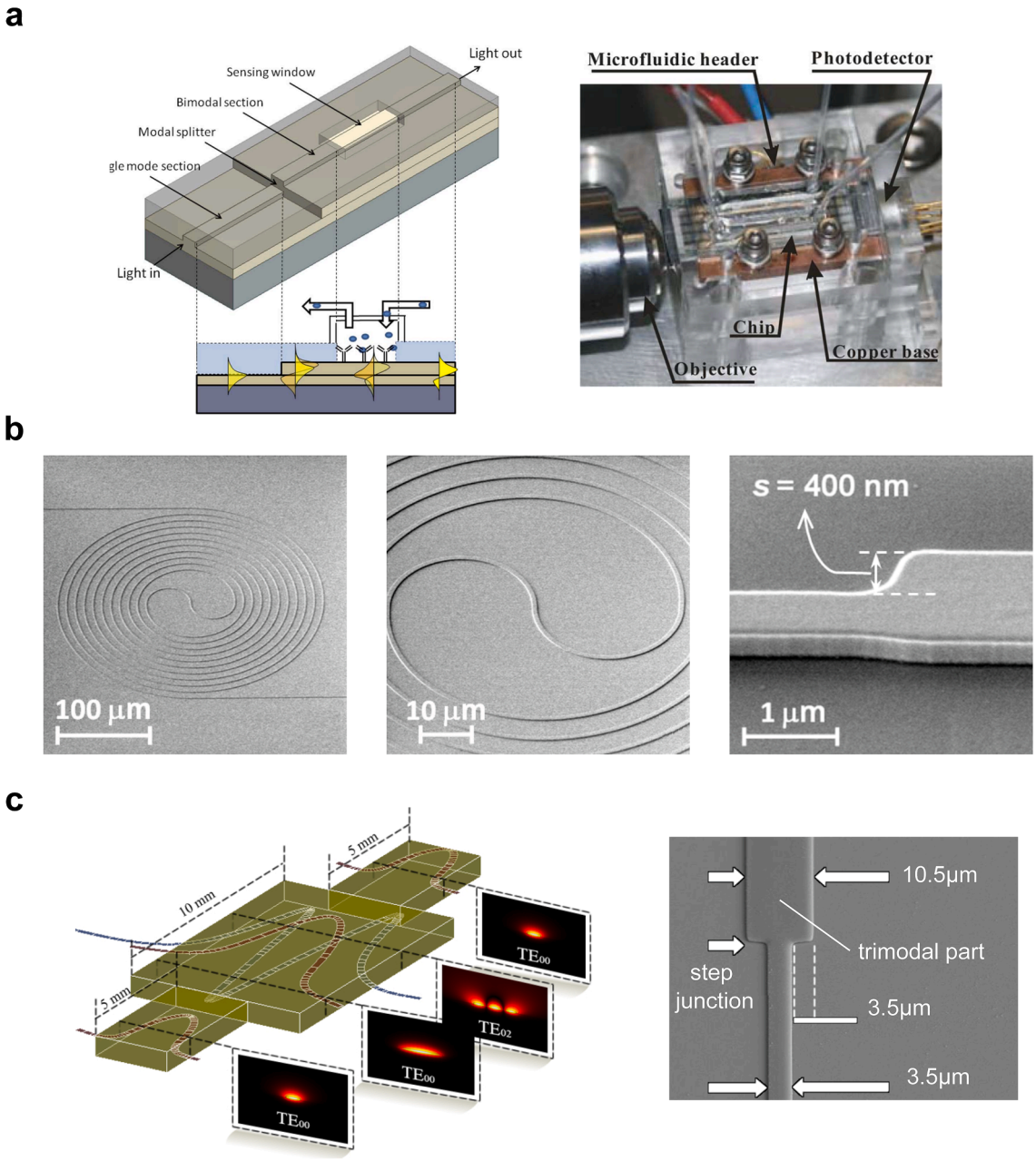

Fig. 3. Types of uniform BiMW sensors: (a) Silicon nitride configuration based on vertical modal splitter and differential detection. Adapted with permission from (Zinoviev et al., 2011) © IEEE 2022. (b) Spiral silicon scheme with horizontal modal splitter. Adapted with permission from (Liu et al., 2014) © The Optical Society 2022. (c) Trimodal low-cost polymer-based waveguide with horizontal modal splitter.
Adapted from Ramirez et al., 2019

presents a thickness of 150 nm and 350 nm in the single-mode and bimodal parts, respectively, for obtaining a response of more than 70 % modulation. They were fabricated using standard microelectronics technology by conventional photolithography processes over 2 μm thermally grown thick silicon dioxide cladding layer and depositing the core layer of silicon nitride by low-pressure chemical vapor deposition (LPCVD) technique. These sensors were reported to have a bulk sensitivity of 1,350 2π rad/RIU cm by using a photodetector attached to the bimodal output facet. As a result, the interference bimodal pattern was directly detected without merging again both modes in a single-mode output waveguide, and falsely interpreted results can be obtained in real biosensing experiments. However, it is worth noticing that although these BiMW can be integrated in compact structures, they are designed in very long optical waveguides to enhance the sensitivity. To mitigate some of these integration limitations, interferometric biosensors based on two-lateral mode spiral silicon waveguides were proposed on SOI wafers patterned by deep UV lithography, Fig. 3b (Liu et al., 2014). The use of horizontal modal splitters simplifies the fabrication process as only a single lithography etching step is required. The width of these structures is found to be 450 nm and 900 nm in the single-mode and bimodal part, respectively. Nonetheless, the bulk sensitivity reported is 504 2π rad/RIU cm, more than half the standard BiMW in silicon nitride, although in a more compact footprint. Similarly, low cost BiMW were reported in the literature by using optical polymer platforms fabricated by soft UV nanoimprint lithography which are transparent at both visible and infrared wavelengths (Liang et al., 2019), and with waveguide designs of 2 μm width in the bimodal part. The phase sensitivity reported in this case is 316 2π rad/RIU cm, although the spectral sensitivity of 789 nm/RIU is more competitive compared to other types of resonant-based IO sensors. Here horizontally confined modes are considered to design the BiMW, as in the previous case, so that fully etched steps are needed in the fabrication processes of the polymer, which drastically reduces costs compared to previous configurations. At the same time, trimodal polymer waveguides fabricated using direct laser writing at 405 nm wavelength were introduced by changing the standpoint of conventional BiMW (Ramirez et al., 2019; Ramirez et al., 2015). Here the second higher order mode with even parity is excited in the bimodal part because of symmetry conditions with the input single-mode waveguide, see Fig. 3c. Since this mode is highly sensitive for cladding variations, high-performance, low-cost SU-8 polymer platforms are demonstrated for sensing applications, reporting bulk sensitivities up to 1366 2π rad/RIU cm in a fully etched and low-cost biosensor with waveguide dimensions in the bimodal section around 10 μm and 12 μm (Liang et al., 2018).

On the other hand, some of the problems that usually must be addressed when dealing with BiMW sensors are related to the excitation of the modes. These must be equally excited so that the modulation depth is increased, which is desirable to obtain a clear read-out signal in the sensing process. To this end, grating assisted BiMW have been introduced providing full control over the power distribution in the waveguide mode resulting in nearly lossless mode conversion (Bruck and Hainberger, 2014). Likewise, vertical polymer tapers are reported for efficient light-coupling in BiMW biosensors to enhance the coupling of collimated or divergent beams (Grajales et al., 2019), as well as novel algorithms to overcome ambiguities that commonly arise from read-out signals typical of interferometric sensors (Bassols-Cornudella et al., 2022).

2.3. Periodic structures

Light propagation through periodically patterned waveguides is feasible under certain conditions. To understand the behavior of light in periodic media, we must first study how the modes evolve for different wavelengths, see the dispersion diagram of Fig. 4. Here, the ratio between the wavelength (λ) and the periodicity of the structure (a) is key as it determines whether reflections are produced or not at the interface in between the periodic elements (Joannopoulos et al., 1997). For a given period, if the wavelength is too large to avoid reflections, we may say we are working in the SWG region. A first approximation to determine whether we are at the SWG regime is considering the next expression: $n_{eff} < \lambda/2a$, where n_{eff} is the effective index of the propagating mode. If this condition is fully met so that the effective index is drastically smaller than the second part of the equation, the periodic waveguide works in the deep-subwavelength region, and it can be modelled as a uniform structure with a pitch much smaller than its wavelength (Cheben et al., 2018). IO biosensors made of SWG structures provide several

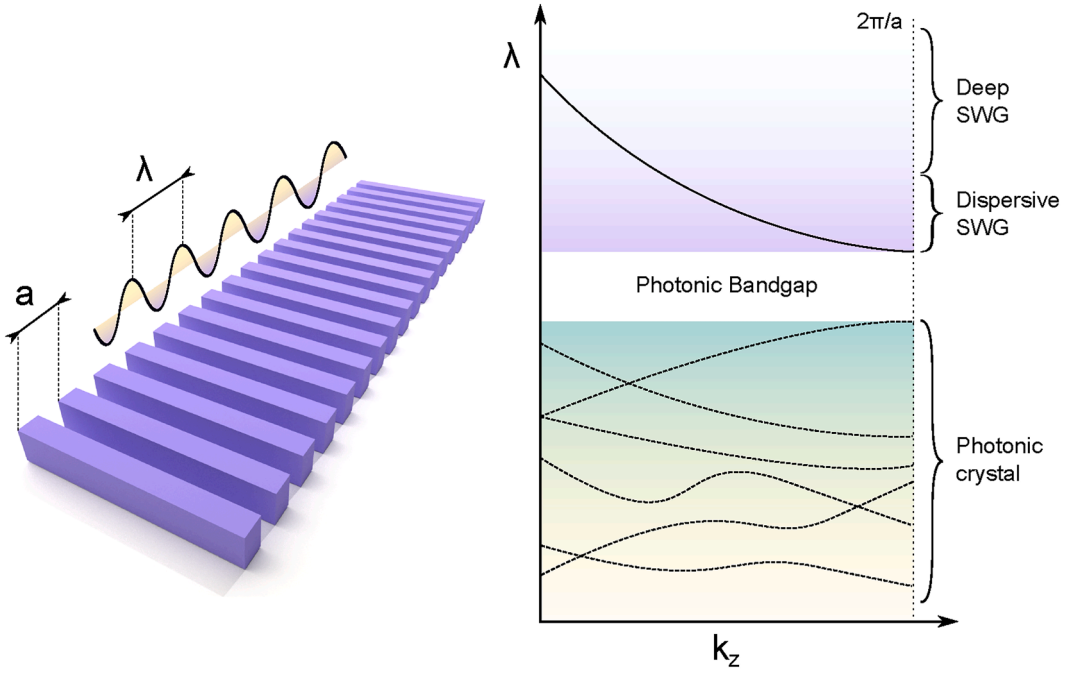

Fig. 4. Periodic waveguide representation and schematic of its dispersion diagram where two main regions are distinguished: subwavelength grating and photonic crystal.

advantages in terms of sensitivity due to the stronger light-matter interaction with the substance of interest (Wangüemert-Pérez et al., 2019). As a result, several conventional spectral-based sensing structures were redesigned using SWG elements for high-performance operation. This is the case of ring resonators made of SWGs with reported sensitivities up to 580 nm/RIU (Flueckiger et al., 2016; Luan et al., 2019). Likewise, BiMWs made of deep SWG elements have been also explored in the literature for biosensing, as it is the case of the perforated silicon nitride waveguide, fabricated using LPCVD, which consists of an array of circular holes about 160 nm diameter formed in the bimodal part of the structure of height 300 nm and width 800 nm, see Fig. 5a (Uchiyamada et al., 2019). However, as we approximate to the PC regime by increasing the periodicity or reducing the wavelength, properties such as dispersion and anisotropy appear and must be considered when designing the SWG waveguides. For instance, the typical dispersion of SWGs has been extensively explored to develop directional couplers (Wang et al., 2016) and beam splitters (Halir et al., 2016) for ultra-broad-band operation in very compact devices. Similarly, the dispersion of SWG can be used to design highly sensitive spectral-based BiMW biosensors, with reported sensitivities up to 2,270 nm/RIU in silicon-based devices fabricated using electron beam lithography, see Fig. 5b (Torrijos-Morán et al., 2019). Dispersion engineered structures with a period of 260 nm and bimodal width of 1.4 μm are herein conceived to provide a similar dispersion for both modes. This is translated into an almost constant phase shift as a function of wavelength that provides critical sensitivity points in interferometric-based sensors (Levy et al., 2009; Levy and Ruschin, 2008). In these configurations, the spectral-based sensitivity can be expressed as

$$S = \frac{\partial \lambda}{\partial n_c} \tag{4}$$

where $\partial\lambda$ is the wavelength shift of a certain spectral feature and for a given change in the bulk cladding refractive index ∂n_c. Considering a SWG-based BiMW and that we work on a spectral peak (either constructive or destructive interference) we can rewrite Eq. (2) as

$$\Delta\varphi = \frac{2\pi L}{\lambda}\eta = N\pi \tag{5}$$

where η is the effective index difference and N is an integer number, even in the case of constructive interference and odd for the destructive case. Using implicit function differentiation, we can calculate the phase derivative respect to the cladding refractive index as follows

$$\frac{\partial \varphi}{\partial n_c} = \frac{2\pi L}{\lambda}\frac{\partial \eta}{\partial n_c}, \tag{6}$$

and respect to the wavelength as

$$\frac{\partial \varphi}{\partial \lambda} = \frac{2\pi L}{\lambda}\left(\frac{\partial \eta}{\partial \lambda} - \frac{\eta}{\lambda}\right) \tag{7}$$

so that dividing Eq. (6) by Eq. (7) we obtain an expression of the spectral sensitivity as a function of the phase shift φ, the effective index differences η and wavelength λ:

$$S = \frac{\partial \lambda}{\partial n_c} = \frac{\partial \varphi / \partial n_c}{\partial \varphi / \partial \lambda} = \frac{\partial \eta}{\partial n_c} \Big/ \left(\frac{\partial \eta}{\partial \lambda} - \frac{\eta}{\lambda}\right). \tag{8}$$

From this equation we can conclude that the sensitivity becomes

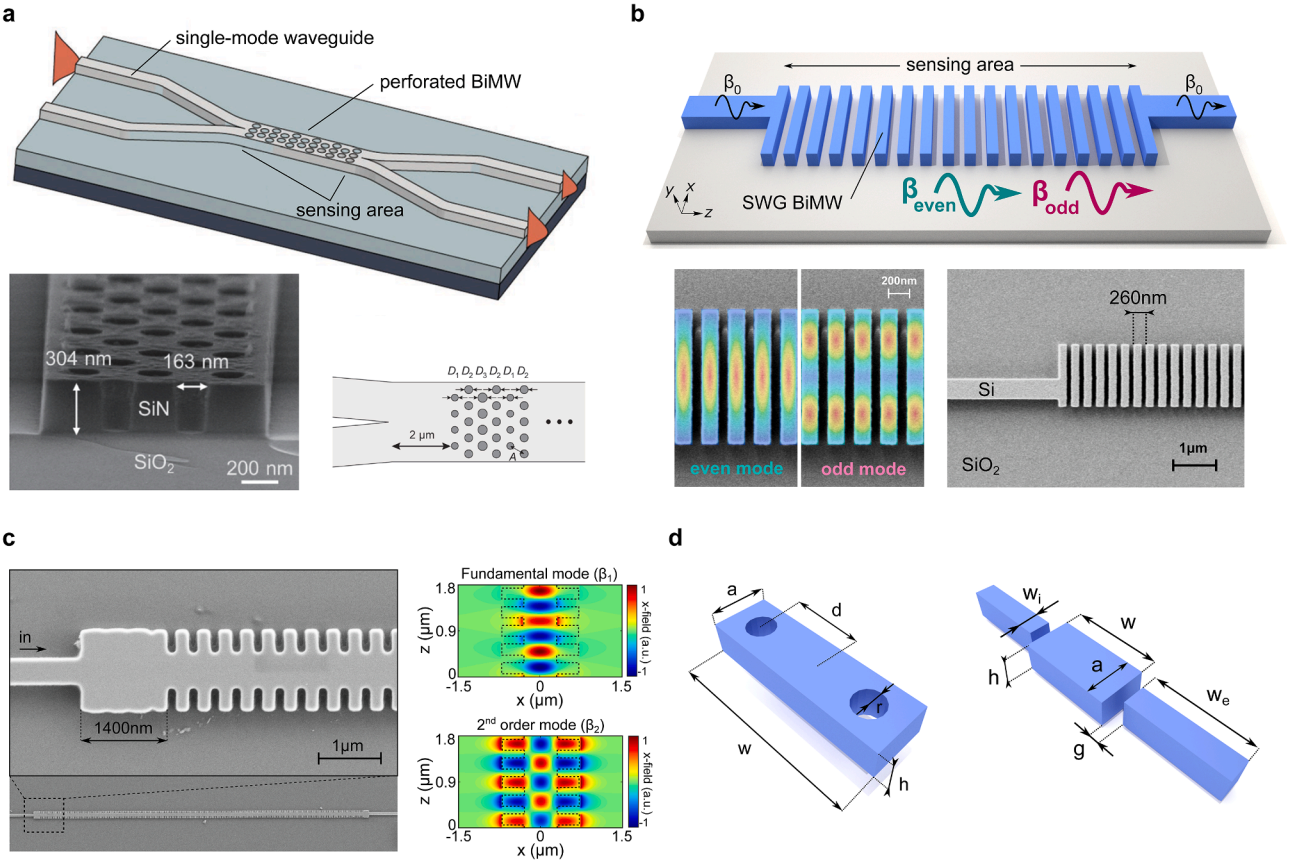

Fig. 5. Types of periodic BiMW sensors: (a) perforated silicon nitride interferometer. Adapted from (Uchiyamada et al., 2019). (b) SWG spectral-based configuration. Adapted with permission from (Torrijos-Morán et al., 2019) © The Optical Society 2022. (c) 1D PCs with high group index contrast made of corrugated waveguides. Adapted from (Torrijos-Morán et al., 2021). (d) Array of patterned circular holes and multi box-based designs. Adapted with permission from (Torrijos-Morán and García-Rupérez, 2021) © The Optical Society 2022.

theoretically infinite when the slope of the phase as a function of wavelength reaches zero. This condition is met at the critical sensitivity point:

$$\frac{\partial \eta}{\partial \lambda} = \frac{\eta}{\lambda}. \tag{9}$$

Dispersive SWGs provoke this behavior in BiMW interferometers, which in addition to the stronger light-matter interaction explains the extremely large sensitivity results obtained by these structures. It is also worth noticing that the duty cycle of the SWG structure is crucial to have an active control of the critical working point, as it determines the phase shift slope evolution, reported optimized values of duty cycle are around 60 % (Torrijos-Morán and García-Rupérez, 2019). Moreover, as it is shown in Eq. (8), the spectral sensitivity does not depend on the sensor length, so that very short interferometric schemes can be designed. The reported spectral sensitivity is notably higher than for other silicon biosensors based on resonant configurations and comparable to plasmonic devices, thus confirming the high potential of SWG bimodal waveguides for label-free biosensing.

As it is depicted in Fig. 4, in the SWG regime the fundamental mode becomes dispersive as it nears the photonic bandgap (PBG) region, where optical modes cannot be propagated through the structure due to Bragg reflections at each interface of the periodic waveguide (Pérez-Armenta et al., 2020). Here both modes are sensitive, and somehow they cancel each other so that almost no phase shift is accumulated at the output. To improve the phase sensitivity, the fundamental mode is supposed to be isolated from changes in the environment, and the higher order mode to be dispersive. This new approach is feasible when dealing with periodic structures below the PBG, in the PC region, where optical modes couple with each other in the dispersion diagram (see Fig. 4) and regions of high group index can be obtained, the so-called slow light regions (Krauss, 2007; Baba, 2008). PCs have been widely demonstrated as biosensors by taking advantage of slow light effects, as in the case of two-dimensional periodic structures made of circular holes and one-dimensional PCs based on corrugated waveguides (Castelló et al., 2012; Sabek et al., 2018; Sabek et al., 2019). The latter present a reduced lateral size compared to other PCs which reduces the final footprint and fabrication complexity while preserving the slow light benefits. In fact, similar 1D PCs have been incorporated in one of the arms of a MZI to design slow light interferometers (Brimont et al., 2011). The underlying mechanism relies on improving the phase shift accumulated by the PC arm due to the slow light phenomena without the need of increasing the length of the interferometer. As a result, very compact MZI schemes are therein designed (Nguyen et al., 2012). A similar device inserting a highly dispersive 1D PC made of circular holes in one of the MZI arms is demonstrated for high-performance biosensing with phase sensitivity values of 13,370 2π rad/RIU cm. In this context, a novel approach was introduced by encompassing the ideas of PCs in MZIs and BiMWs (Torrijos-Morán et al., 2021). This is the case of the slow light BiMW fabricated using electron beam lithography in a 1D PC for high-performance interferometric operation, see Fig. 5c, where sensitivities of 10,620 2π rad/RIU cm are demonstrated in single-channel compact structures with a period of 370 nm and bimodal waveguide width of 1400 nm. The fundamental and the second order mode both with even parity are herein excited as in the case of the trimodal waveguide, but now in a highly dispersive 1D PC so that the design dimensions are reduced. In order to critically enhance the phase shift in the bimodal interferometer, the group index of the higher order mode is drastically increased compared to the fundamental one. On this matter, PCs allow us to engineer bimodal interferometers with high group-index-contrast waveguides by a proper design of the unit cell and thus its dispersion diagram. In this case, the interferometers are exploited to exhibit a large phase shift at the output, similar to other BiMWs and contrary to SWG bimodal configurations where the spectral-based sensing is optimized. Similarly, slow light BiMWs exciting the fundamental and the first high-order mode are also demonstrated as 2x2 switches in really compact footprints and with very low power consumptions (Torrijos-Moran et al., 2021). Besides, different geometries are further investigated as high group-index-contrast single-channel interferometers for all kind of IO purposes, which demonstrates the impact of these BiMWs beyond sensing applications (Torrijos-Morán and García-Rupérez, 2021). Note also that the bimodal excitation must be addressed when dealing with junctions between uniform and periodic waveguides that could negatively affect the device performance (Zhao et al., 2017).

Table 1 shows a detailed comparison of all aforementioned configurations. Examples of classical interferometric sensors based on Young (Schmitt et al., 2007) and Mach-Zehnder (Prieto et al., 2003) interferometers are also included for the sake of comparison. The former presents the lowest detection limit although the read-out measurement is carried out off-chip and additional optical components are needed. MZIs have been in turn the standard interferometric sensing configurations over the years due to their ease of design, performance and on-chip measurement. For the case of BiMW configurations, we may highlight that the periodic configurations (SWG and slow light) exhibit the highest bulk sensitivities both in terms of spectral and phase shift, respectively. In detail, SWG BiMW provides a sensitivity 3 times higher than low-cost BiMW, and slow light configuration more than 7 and 10 times higher than vertical BiMW, and conventional MZIs, respectively. However conventional vertical BiMW presents a better detection limit than the other BiMW configurations, due to the read-out stabilization and low noise, which is highly desirable for biosensing. This is mainly due to the optimization of the modal excitation in the case of the uniform BiMW which produces a low-noise read-out signal. In contrast, the periodic BiMW is much noisier because of the cavity formed in the bimodal part, which produces some ripple in the read-out signal. In order to reduce the noise of periodic configurations and thus maximize the detection limit, further optimization in the bimodal excitation must be addressed, specifically in the field mismatch between the fundamental mode at the input and the higher order mode in the periodic waveguide. Another interesting next step would be designing these periodic configurations in silicon nitride, as in the case of the perforated BiMW. This material platform provides a lower refractive index contrast than SOI, so that the light-matter interaction is enhanced, which could be beneficial both in terms of sensitivity and detection limit. It should be also noted that the sensing length is drastically reduced in the case of the periodic configurations compared to the uniform ones, which demonstrates the high potential in the integration of multiple devices in a single chip. However, the fact that the sensing performance of BiMW based on periodic structures depends on their dispersive behavior makes that their optimal operation bandwidth is reduced to few tens of nanometers. Additionally, the need of exciting higher order modes of the periodic structure in order to achieve the required interferometric behavior can also have an effect on insertion losses, although they can be kept below 1–2 dB if a proper design of the access coupling elements is carried out.

3. Lab-on-a-Chip integration and biosensor applications

In view of the exceptional sensing performance provided by BiMW interferometers, their application for biomedical and environmental sensing holds a great potential toward the advanced on-site testing. The implementation of BiMW technologies as portable and multiplexed POC biosensors would offer rapid one-step analysis, minimum reagent consumption, and high reliability and accuracy. However, the development of fully operative POC biosensors must tackle certain challenges in terms of optical system engineering, microfluidics design, and surface biofunctionalization. Hereunder, we will discuss the latest advances in this regard, and will give an overall perspective of the achievements in the demonstration of BiMW biosensors as analytical tools for medical diagnostics and environmental control.

Table 1
Comparison of different types of interferometers, including BiMW biosensors. The most important parameters discussed in this review are shown. N.D. means not determined by the author.

Configuration	Bulk sensitivity	Detection limit	Modal symmetry	Modal splitter	Material platform	Sensing length	Ref.
Young	$dn_{eff}/dn_c = 0.22$	9×10^{-9} RIU	Single-mode	none	Ta_2O_5	5 mm	(Schmitt et al., 2007)
MZI	966 2π rad/RIU cm (Phase shift)	7×10^{-6} RIU	Single-mode	none	Si_3N_4	15 mm	(Prieto et al., 2003)
Vertical BiMW	1,350 2π rad/RIU cm (Phase shift)	2.5×10^{-7} RIU	Even/odd	Vertical	Si_3N_4	15 mm	(Zinoviev et al., 2011)
Spiral BiMW	504 2π rad/RIU cm (Phase shift)	2.2×10^{-5} RIU	Even/odd	Horizontal (full-etch)	SOI	4.5 mm ($185 \times 185\ \mu m^2$)	(Liu et al., 2014)
Low-cost BiMW	789 nm/RIU (Spectral shift)	N.D.	Even/odd	Horizontal (full-etch)	Polymer (Ormocore)	5 mm	(Liang et al., 2019)
Trimodal BiMW	1,366 2π rad/RIU cm (Phase shift)	N.D.	Even	Horizontal (full-etch)	Polymer (SU-8)	15 mm	(Liang et al., 2018)
SWG BiMW	2,270 nm/RIU (Spectral shift)	2×10^{-5} RIU	Even/odd	Horizontal (full-etch)	SOI	0.125 mm	(Torrijos-Morán et al., 2019)
Perforated BiMW	194 nm/RIU (Spectral shift)	20.4 μm/mL (Surface DL)	Even/odd	Horizontal (full-etch)	Si_3N_4	0.1 mm	(Uchiyamada et al., 2019)
Slow light BiMW	10,620 2π rad/RIU cm (Phase shift)	6.6×10^{-6} RIU	Even	Horizontal (full-etch)	SOI	0.078 mm	(Torrijos-Morán et al., 2021)

3.1. Integration in lab-on-a-chip (LOC) platforms

The engineering of photonic biosensor systems must address several parameters, such as the light in-coupling, optical read-out, data processing, and microfluidics integration for sample transport and analysis. Selection of the most appropriate light sources and detectors, their miniaturization and incorporation in robust devices – ideally with a low cost –, and the accomplishment of high-efficient and high-resolution read-outs are probably the biggest challenges in photonic waveguide biosensor development. Table 2 summarizes the main advantages and limitations of different optical components.

Different light sources that can be used for BiMW interferometric operation include light emitting diodes (LEDs), diodes bars, and laser diodes, being the last ones the most widely employed. Main technical requirements are the narrow band emission and a directional mode, while low power consumption and low cost might be preferred for implementation in POC biosensors. Further, the light source must be precisely aligned and coupled to micrometer-sized waveguides, and in multiplexed sensing, simultaneously illuminate different waveguides. In order to incorporate a single light source in a multiplex chip, beam splitters such as Y-branches (Aikio et al., 2015) or multimode interference branches (MMI) (Guo et al., 2021) are presented as possible microfabrication approaches. Beam splitters generate uniform power splitting along the several waveguide branches from the input interface. The MMI coupler, compared to a matrix of Y-junctions, offers advantages in terms of compactness. Nonetheless, these branches suffer from propagation losses along the path of light hindering an efficient light coupling. Diode arrays (Laser Diode Technology, n.d.; Shimizu et al., 2014) are an alternative approach to the use of beam splitters as they do not require any extra fabrication process on the chip waveguides. An example of integration of diode arrays in PICs was shown by Theurer *et al.* (Theurer et al., 2020), where the diode, with an optical power of 60 mW, demonstrated coupling loss of 2.1 dB in silicon nitride waveguides. They employed a hybrid flip-chip integration interface method, which resulted to be an efficient solution for chip integration and being readily adaptable to other platforms. However, restraints such as polarization of the light or tuning of the wavelength for the specific application in BiMW could limit their purpose. In terms of alignment, different solutions have been proposed to achieve compact, simple, easy to built-in and be automated, including grating couplers, tapers, or other free-space in-coupling methods (Son et al., 2018). Grating couplers are composed of periodically spaced diffractive elements and these optical structures diffract the light in such angles that can be defined by the Bragg condition. This coupling method can enable the light entering the waveguide with high alignment tolerances, achieving efficient light couplings although this device must be carefully fabricated with high resolution lithography techniques in order to achieve sub-micron scales (De Vos et al., 2007). Duval *et al.* (Duval et al., 2012) proposed the incorporation of a nanograting coupler directly in the BiMW chip that work under the visible spectrum of light for an efficient light coupling and possible integration at large scale due to the use of standard fabrication processes. In this work, a taper is integrated after the grating coupler to increase coupling efficiency. Waveguide tapers can be lateral, vertical or three-dimensional, employed to increase the waveguide input area and increase the coupling efficiency (Son et al., 2018). Grajales *et al.* (Grajales et al., 2019) reported a low-cost solution for a vertical taper made from SU-8 polymer, fabricated in a wafer level and integrated in the BiMW sensor with three additional photolithographic mask levels, obtaining an experimental coupling efficiency of 55 % corresponding to a coupling loss of 2.63 dB. However, they stated certain fabrication limitations that increase scattering and explain the power loss. This forefront strategies are usually combined with the use of a direct optical fiber light source, which can be mechanically directed and focused on the input waveguide to create a more user-friendly and easier to automatize coupling approach with high efficiency couplers. Collimation and polarization lenses can be easily adapted in the fiber output optics (Son et al., 2018). An avant-garde approach for an automated light in-coupling has been proposed by Morichetti *et al.* (Morichetti et al., 2014) using on-chip photodetectors. These devices measure the intensity of the light inside the waveguide and send signals to a self-configuring system of beam coupler (Miller, 2013; Bogaerts et al., 2020). Results show that light is monitored with a sensitivity of 30 dBm and have demonstrated applications for waveguides. Although one should note that for medical applications it is required to design single-use devices in order to avoid cross-contamination of samples in flow. For this end, optical integration of the different optical building blocks should be accomplished at a small cost in mass fabrication processes.

Finally, the propagated light that exits the BiMW has to be collected by a detector for signal processing and data acquisition. Devices such as two-section photodetectors can be found as a low-cost, easy to configure, and work as miniaturized devices in single waveguide approach. However, the area of the sections and signal–noise ratios can be quite limiting factors in terms of sensitivity of the devices. In terms of multiplexed waveguides, CCD cameras may show improved characteristics, exhibiting extraordinary features in terms of pixel resolution. Single light sensitive areas fabricated in a wide matrix enables processing and control of each waveguide output signal separately, even in low-output power scenarios (Dante, 2014). This signal output is processed

Table 2
Advantages and limitations of BiMW optical schemes for LOC integration.

Device	Advantages	Limitations
Light Source		
Light emitting diodes (LEDs)	Low power consumption Low cost Optically safe	Not directional beam Relatively broad light spectrum Incoherent light
Laser diodes	Low power consumption Low cost High optical efficiency Directional beam Narrow light spectrum Multi-mode operation regime Allows light modulation of light Adaptable to beam splitters and gratings	No circular beam shape Require thermal and electrical controllers Single input interface coupling Can be dangerous for vision
Diode bars	Multi-coupling approach Integration during fabrication	High power consumption No collimated light
In coupling methods		
Free-space laser diodes (Son et al., 2018)	Low cost Requires higher-power light source Robust in laboratory environments	Requires additional optical components Careful alignment of the optical set-up Collimation of light can be challenging Not robust for portable applications
Fiber-coupled laser diodes (Son et al., 2018)	Easy alignment Uniform beam intensity profile Easy integration in optical fibers Compact set-up	Power loss along the optical fiber length
Grating (Duval et al., 2012)	Solution to free-space couplings Allows tuning of the light spectrum	Increased fabrication cost and time Out-of-plane coupling method
Taper (Son et al., 2018)	High efficiency coupling	Located on the chip edges Require chip polishing
Beam splitters -MMI splitters (Guo et al., 2021)	CMOS compatible fabrication Input fiber coupled beam Allows beam polarization Reduction of bulky electronic components	High power laser beams Propagation losses along the light path
Photodetectors		
Photodiode array	Miniaturized device Low cost	Difficult integration in multiplex approach High noise
CCD camera	Low noise and high sensitivity Low light spectral measures Individual control of pixel in the matrix	Bulky component Saturate at low input power Speed of data acquisition

according to the interferometric effect of light in BiMW sensors, in which variations in the phase of light of the two propagating modes produce changes in the oscillation of the light modes. The output signal is measured as a shift of the two light modes in terms of a photon profile distribution, showing a sinusoidal signal at a certain amplitude and time. When a binding event occurs on the sensor surface, the sinusoidal baseline is altered changing its amplitude and frequency as result of the interferometric phase shift. The shift is directly proportional to the refractive index variation occurring at the sensor-dielectric interface, which in turn is directly proportional to the concentration of analyte binding to the surface. Some methods used to quantify the correspondent variation of light phase were based on the number of counts from maximum and minimum values of the periodical wave. Due to complexity and time-consuming method to analyze data, new phase retrieval techniques have been designed. Dante *et al.* (Dante et al., 2015) developed an all-optical modulation technique combined with a Fourier Series deconvolution algorithm to achieve a linear read-out; it allowed a facile implementation by using commercial laser diodes under high-frequency intensity modulation. The technique has been recently improved by Bassols-Cornudella *et al.* (Bassols-Cornudella et al., 2022) with the incorporation of a new modulation algorithm based on simple trigonometric relationships of sinusoidal signals, which could possibly be applied to any type of time-dependent sinusoidal signal. As a result, the sinusoidal interferometric signals are presented as linear responses, which are simpler and more user-friendly to be applied in a POC biosensor device.

Besides optical engineering, the integration of microfluidics into the biosensor system is of high importance as it allows for a minimum sample consumption and manipulation, and dynamic and automated injection and washing steps. The fabrication of such microfluidic platforms is complex due to the reduced size of the channels, the need of channel interface alignment, and the integration of fluidic manipulation modules for automated sample delivering (and processing) in a flexible and scalable platform (Zeming et al., 2016). Concerning the type of materials, polydimethoxysiloxane (PDMS) is the most widely used material for this application as it is biocompatible, robust, transparent, and low-cost material (Yavas et al., 2017). In order to achieve an automated platform integrated with photonic biosensors, it has been reported the use of digital microfluidics (Ceyssens et al., 2013), droplet-based microfluidics (Hess et al., 2020), or micromechanical valve based microfluidic systems (Yavas et al., 2017; Aćimović et al., 2014; Szydzik et al., 2017; Parks et al., 2014; Cai et al., 2015; Schudel et al., 2009; Ceyssens et al., 2013). Among these, the micromechanical valves have achieved the highest interest for fluidic automation of photonic biosensors. Szydzik *et al.* (Hess et al., 2020) reported an example of an automated microfluidic system containing different modules in a single PDMS device (i.e., six fluidic reservoirs connected to the primary channel through different pneumatic valves, waste channel). Each primary fluidic channel is 250 μm wide and they have automated the pressure regulation for −900 mbar in actuation and + 50 mbar for valve closure. However, this module only contains a single channel (Fig. 6a). Other platforms containing similar valves have been developed, as shown by Acimovic *et al.* (Szydzik et al., 2017) they have incorporated eight sensing channels each of them can be controlled individually or simultaneously, their work was tested in a clinical application in a photonic device showing real-time measurements (Fig. 6b). On the other hand, an important function of microfluidic systems for point-of-care applications is sample pre-treatment (e.g., separation of plasma from whole blood). Recent developments in this field have been done focusing on automated platforms to be simply integrated in point-of-care setting as reliable, safer, and faster approaches. A filtration platform was reported by Lenz *et al.* (Lenz et al., 2021) in which they describe as being a low-cost device, for processing small volumes of whole blood (90 μL) and offering minimal loss of sample integrity. This device achieved an ideal spinning velocity of 4500 rpm (during 3 min) for a serum separation with few red blood cells when compared with traditional centrifugated serum (Fig. 6c). Apart from these examples, many other solutions have been developed and demonstrated not only in optical biosensors but for fluorescent microarrays or other lab-on-a-chip devices, which could motivate their eventual incorporation in BiMW systems, boosting their exploitation and application in real bioanalytical scenarios.

3.2. Sensor biofunctionalization

In label-free sensing, the analytical sensitivity and specificity ultimately depend on the biorecognition element and how it is tethered on the sensor surface. Typically, most employed bioreceptors are antibodies and nucleic acids (i.e., DNA probes), although other molecules such as aptamers, cell receptors, or polymers can also be used. These

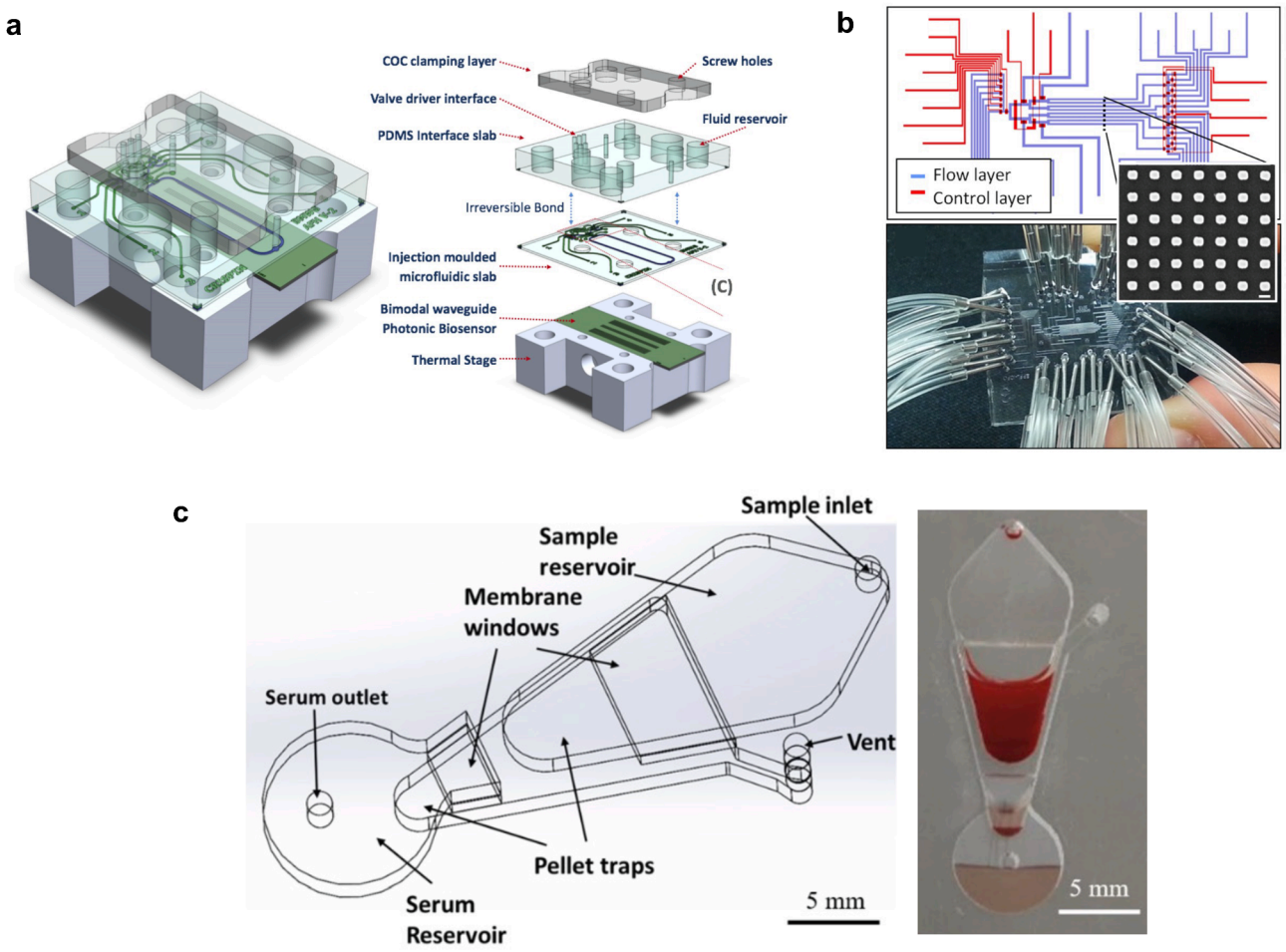

Fig. 6. Schematics of automated microfluidic devices: (a) single channel microfluidic platform fixed to the BiMW biosensor. On the right, the model shows the PDMS interface slab bonded irreversibly to the injection platform and a clamping layer. Reproduced from (Hess et al., 2020) with permission from the Royal Society of Chemistry. (b) Schematics of the flow and control layer of a multiplex microfluidic chip containing 8 flow channels. Image of the connected chip below. Adapted with permission from (Szydzik et al., 2017) © American Chemical Society 2022. (c) Portable filtration unit successful separates serum from blood in different reservoirs by centrifugal forces. On the left is the schematic of the device, containing multiple channels stacked on top of each other and separated by membrane windows. Adapted from (Lenz et al., 2021).

bioreceptors show extraordinary affinity and specificity towards their corresponding analyte, allowing the selective capture of the target with a high sensitivity. However, the immobilization procedure on the sensor surface must take into account several parameters, such as the stability, the grafting density, the orientation, and the minimization of non-specific adsorption of other substances present in the sample matrix.

Commonly, the sensor surface biofunctionalization consists in the chemical modification of the silicon-based waveguide for the immobilization of the appropriate bioreceptors. This chemical modification is carried out through the so-called silanization. This procedure employs reactive alkoxysilane molecules to form a self-assembled monolayer onto the silicon surface that display functional end groups (e.g., amine, carboxyl, etc.) at the outer interface (Soler and Lechuga, 2022). A wide variety of protocols have been described to achieve a reproducible silanization reaction on silicon surfaces, including liquid and vapor phase reactions (Luchansky and Bailey, 2012). As an example, for the case of the amino-functional silanes such as (3-aminopropyl) triethoxysilane (APTES) the protocol can occur in solution with anhydrous toluene (Moon et al., 1996), or with chemical vapor deposition (CVD) at room temperature for 4 h (Giraud et al., 2016), or CVD at 150 °C for 5 min (Zhang et al., 2010). The in-solution reactions are prone to result in low ordered or multilayer coatings (González-Guerrero et al., 2013), therefore some protocols refer to the use of vapor-phase deposition combined with measure tools for tracking the deposition rate with high precision and reproducibility (Luchansky and Bailey, 2012; Huang et al., 2012). Additionally, some strategies have been applied to enhance the antifouling properties of the silanized surface, such as the incorporation of polyethylene glycol (PEG) groups in the silane chain (Maldonado et al., 2020). These molecules offer a high resistance toward non-specific adsorptions by creating a hydration layer on the surface, being therefore useful when attempting direct measurement of complex biological fluids (Soler and Lechuga, 2022). Nonetheless, the main issue with silanization is the lack of a standardized and universal protocol to be applied in all type of silicon sensors, as it highly depends on the silicon surface quality, ambient conditions, solvents, temperatures, etc.

Upon surface modification, the immobilization of the bioreceptor must also be optimized in terms of stability, orientation, and grafting density. Conventional strategies are based on the covalent binding of the biomolecules to the functional silane layer via cross-linking reactions. A myriad of chemical crosslinkers is available for the covalent binding of receptors to the modified surface via amine–amine, amine-carboxyl, thiol-amine, or thiol-thiol binding, among others (Fig. 7b). This covalent binding method offers important advantages such as the high stability of the bioreceptor layer and the control of the bioreceptor density by tailoring the number of functional groups or including lateral spacers. However, it generally occurs randomly, without any preferred orientation. To ensure an oriented immobilization of bioreceptors, it is possible to make use of affinity ligands, such as protein A or protein G, that bind

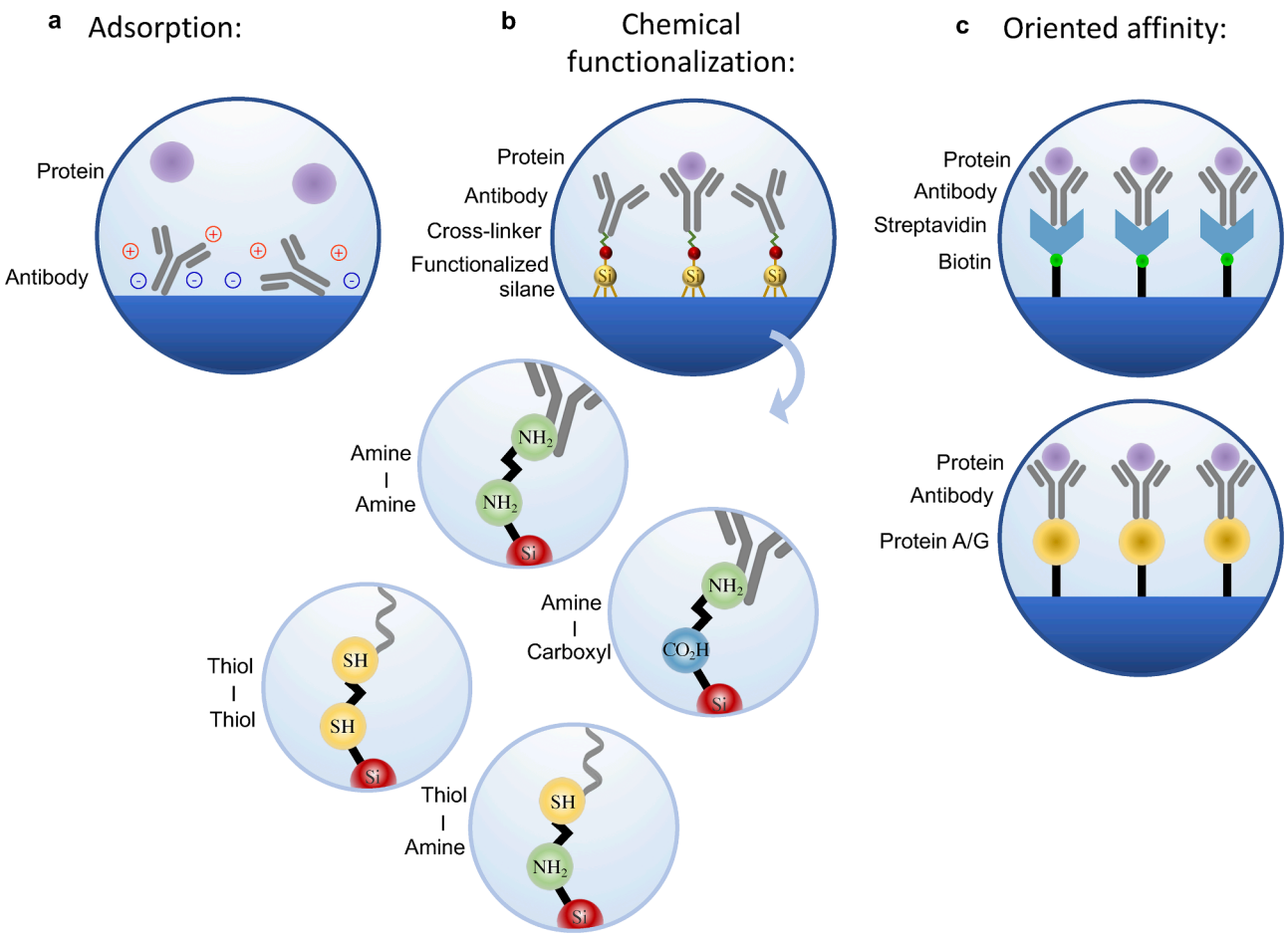

Fig. 7. Schematics of different surface biofunctionalization approaches for bioreceptor immobilization: (a) physical adsorption of bioreceptor through electrostatic forces, offers poor orientation for analyte specificity; (b) chemical functionalization employed for strong bond of the bioreceptor on surface, using functionalized silanes to immobilize bioreceptor through chemical bonds of crosslinking reactions. Different type of chemical bonds illustrated, using amine cross-linkers and thiol cross-linkers; (c) biotin/streptavidin pair or the use of protein A/G are mostly employed to achieve oriented affinity of the bioreceptor on surface.

antibodies through their constant region, or the use of biotin/streptavidin pair (Fig. 7c) (Gunnar and Carl-Fredrik, 2011; Freitag et al., 1998).

On the other hand, innovative approaches have also been developed for the application of BiMW technologies as chemical and gas sensors. Herein, the recognition interface typically consists in chemical matrices, such as graphene (Yavari et al., 2011) or carbon nanotubes (Modi et al., 2003) able to selectively capture small organic or gas molecules. Recently, the use of highly porous coatings of Metal-Organic Frameworks (MOFs) has also been achieved. Tao *et al.* (Tao et al., 2017) report the use of zeolitic imidazolate framework-8 (ZIF-8) film due to its high surface area, good water stability and efficient light transmittance. They deposited ZIF-8 layer by layer with an intergrowth process above the entire chip. The final pattern on the waveguide was done with lithography and chemical etching (Fig. 8 a-c). The activation of the MOF film is done by immersion in anhydrous methanol for 3 days for the release of unreacted species. The film is then dried under a dynamic vacuum for 12 h, reaching a thickness of ZIF-8 coating around 1 μm. Chocarro-Ruiz *et al.* (Chocarro-Ruiz et al., 2018) also report the application of ZIF-8 nanoparticles for coating of the BiMW waveguides (Fig. 8 d-f). Their deposition method consisted of spin-coating of the ZIF-8 solution, evaluating the desired nanoparticles concentration and spinning speeds. They achieved 90 % light transmittance on surface and showed 100 % gas sensor response.

3.3. Applications in biomedical and environmental analysis

BiMW biosensors can be used in a wide range of applications in both the biomedical and environmental areas. In medicine, biosensors are introduced as analytical tools for diagnosis and prognosis of a disease, as well as to monitor the treatment progress through the selective detection of specific biomarkers in the body fluids. Most common biomarkers are proteins and enzymes, as well as genomic molecules, such as microRNAs. A few examples have been reported demonstrating and, in some cases, validating the BiMW biosensor technology for clinical purposes.

One of the first works was published by Gonzalez *et al.* (González-Guerrero et al., 2017) reporting the detection of the human growth hormone (hGH) in urine samples as a non-invasive method for diagnostics of acromegaly disease. The bioassay was based on the direct interaction of antibody-antigen and different concentrations of hGH were tested in buffer urine sample and clinical validation was done with human spiked urine samples. The results show a limit of detection for spike urine sample of only 3 pg/mL. The same BiMW biosensor was applied for the diagnostic of bladder cancer through the direct detection of a specific microRNA marker also in urine samples (Fig. 9a) (Huertas et al., 2016). In this case, an outstanding sensitivity was obtained, reaching a limit of detection of 23 aM, and successfully validating the biosensor with the evaluation of clinical samples from healthy individuals and cancer patients. More recently, the BiMW biosensor has been demonstrated for diagnosis of bacterial infections. Maldonado *et al.* (Maldonado et al., 2016) showed an ultrasensitive detection of

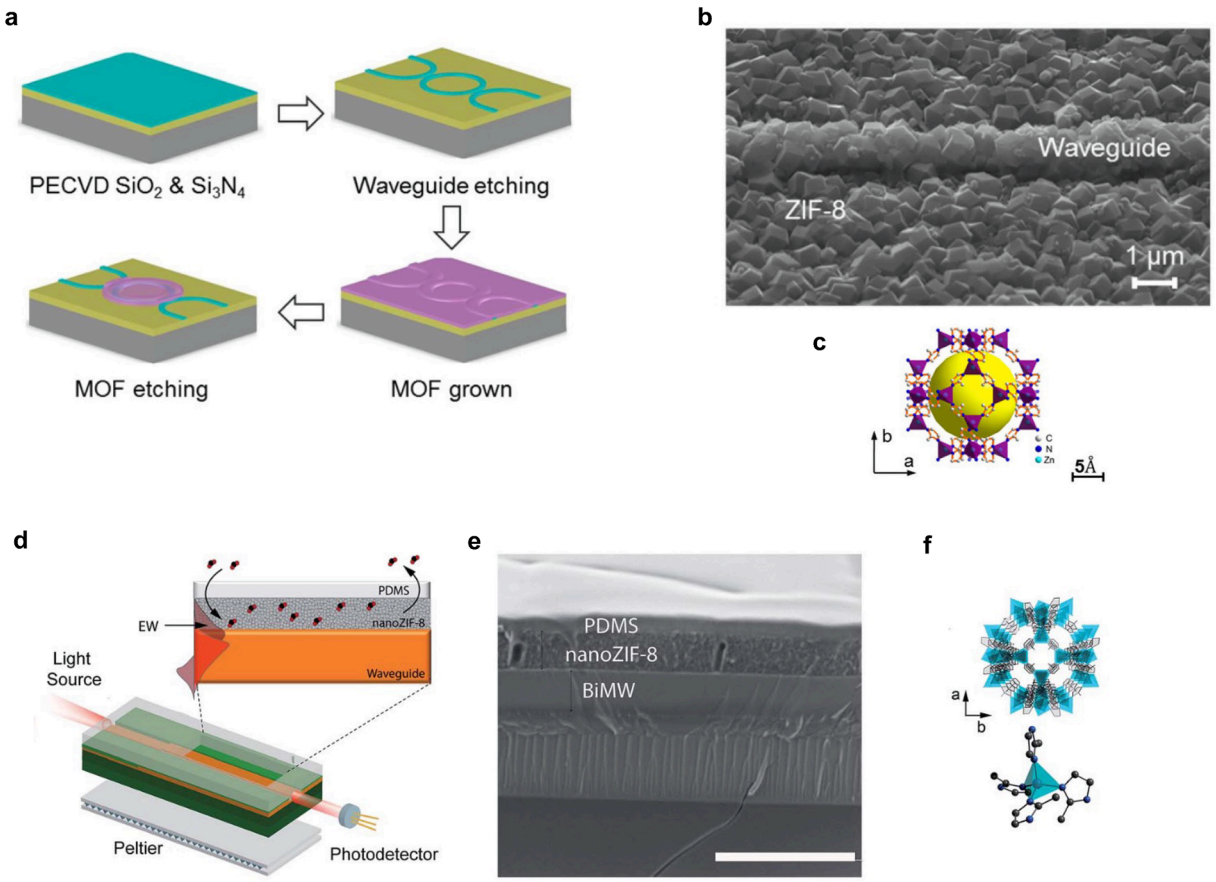

Fig. 8. Surface functionalization using MOFs (a) Photonic resonator - MOF sensor device fabrication process by layer deposition of MOF films. (b) Scanning electron microscope image (top view) of the waveguide containing ZIF-8. (c) Chemical structure of the ZIF-8 nanocrystals. Adapted from (Tao et al., 2017). (d) BiMW sensor device coated with nanoZIF-8. (e) FE-SEM image (side view) of the nanoZIF-8-based BiMW sensor, showing the layers of nanoZIF-8 and PDMS built on top of the waveguide. Scale bar: 5 mm. (f) Structure of the ZIF-8 particle. Reproduced from (Chocarro-Ruiz et al., 2018) with permission from the Royal Society of Chemistry.

Escherichia coli in ascitic fluid of cirrhotic patients, reaching limit of detection of 4 cfu/mL. They also applied the biosensor for detection of hospital acquired infections through the rapid detection of *Pseudomonas aeruginosa* and *Staphylococcus aureus* with detection limits below 50 cfu/mL (Maldonado et al., 2020). Furthermore, they have also been able to identify antibiotic resistance and susceptibility, which is paramount for therapy decision making (Fig. 9b) (Maldonado et al., 2020). Finally, it is worth mentioning that the BiMW system is also being applied for the detection of coronavirus disease (COVID-19) (Fig. 9c) (Ruiz-Vega et al., 2021). In environmental applications, BiMW biosensors have been employed mainly for detection of contaminants and pollutants either in air or waters. For example, the MOF biosensor developed by Chocarro-Ruiz *et al.* (Chocarro-Ruiz et al., 2018) was applied for the detection and quantification of CO_2 gas, which could be used for room contamination measurements. Recently, Ramirez-Priego *et al.* (Ramirez-Priego et al., 2021) demonstrated the real-time monitoring of fenitrothion in tap water samples, achieving a detection limit of 0.29 µg/mL (Fig. 9d).

More novel types of BiMW technologies are also being demonstrated for bioanalytical sensing, although validation with real scenarios has not been fully accomplished yet. For example, Liu *et al.* (Liu et al., 2014) developed a spiral BiMW sensor that demonstrated quantification of biotin-streptadivin interactions over a wide range. The perforated BiMW biosensor described by Uchiyamada *et al.* (Uchiyamada et al., 2019) has been tested with the human serum albumin (HSA) in a surface modified with molecular imprinted polymers in a label-free approach. In this sensor, the detection limit is calculated at 20.4 µg/mL, which is not high enough for its use in urine testing. Similarly, SWG BiMW have been explored in biosensor experiments by Torrijos-Morán *et al.* (Torrijos-Morán et al., 2020) for the recognition of bovine serum albumin (BSA) protein. A concentration of 10 µg/mL of BSA has been detected using protein A/G and antibodies as surface biofunctionalization. These examples confirm that although being still in its infancy, the application of BiMW technologies for biomedicine and environmental control is rising area of research with a promising and attractive future ahead. Efforts should now be directed to attain truly operative LOC systems based on BiMW biosensor that can be integrated in fully automated and user-friendly POC devices to be operated by non-specialized users. Also, research focus should be placed on the sensor biofunctionalization and assay optimization in order to exploit the full potential of the ultrasensitive detection offered by the different and innovative BiMW designs.

4. Conclusions

In summary, this review provides an overview of BiMW biosensors from the fundamentals to its application in LOC devices and detection of real samples. Last advances on the topic are presented and discussed regarding its operating principle, materials employed, detection method and integration capabilities. Specifically, uniform and periodic configurations are studied to develop BiMWs and compared in terms of performance. Uniform schemes are widely demonstrated for different biosensing purposes which shows the high degree of maturity within this area compared to other IO-based devices. In contrast, periodic configurations have been recently proposed and have a long way to go in the biosensing field. Nevertheless, first results show a promising potential as a result of outstanding sensitivity performances (aM-fM range) and highly compact design for integration in portable and user-friendly POC

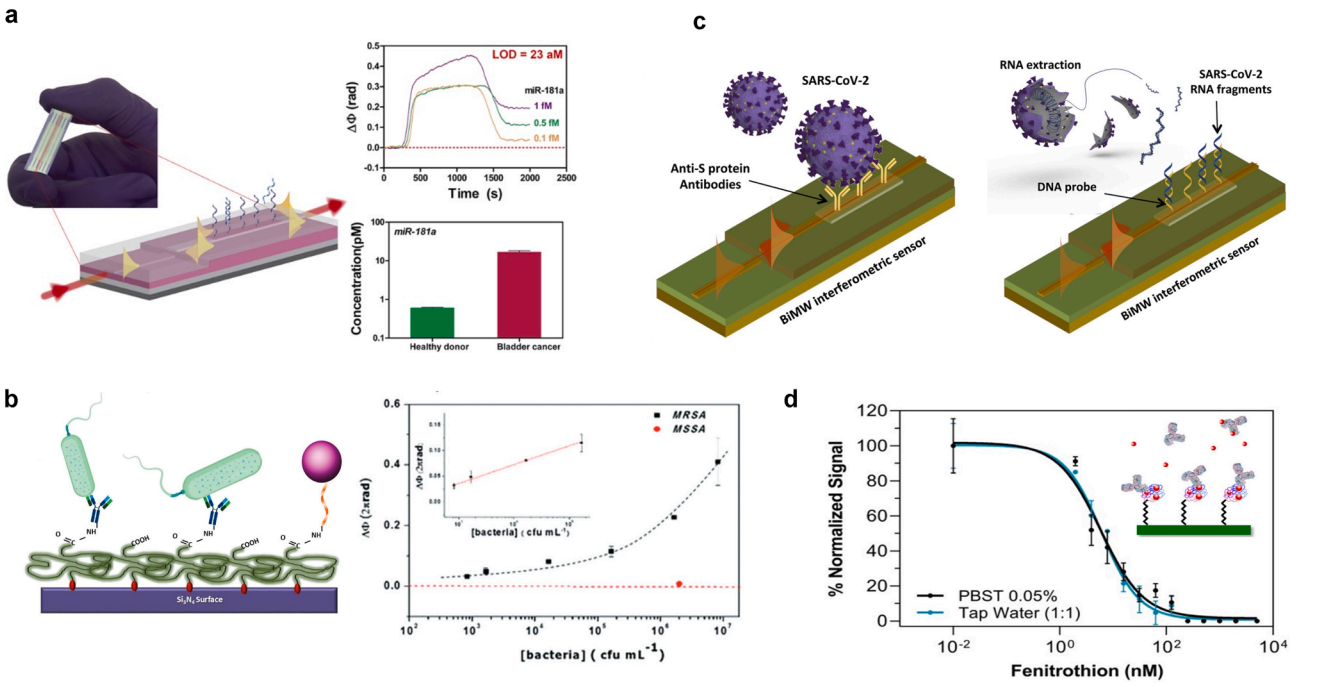

Fig. 9. Applications of the bimodal sensors on biomedical and environmental analysis. a) Bladder cancer patients samples containing selective miRNAs used for the prediction of the disease at attomolar of concentration. Real-time detection of miR-181a at different concentrations. Concentrations of miR-181a in healthy donors and cancer patients. Adapted with permission from (Huertas et al., 2016) © American Chemical Society 2022. (b) Bacteria resistance detections employing a surface of silane-PEG-COOH surface provided a highly specific detection of bacteria (MRSA), while non-specific bacteria (MSSA) was used to demonstrate the microbial-repelling property of the surface. Adapted from (Maldonado et al., 2020). (c) Two strategies used for the SARS-CoV-2 diagnosis with the BiMW biosensor: on the left, the illustration of the intact SARS-CoV-2 virus detection; On the right, the viral genomic material is detected. Adapted from (Ruiz-Vega et al., 2021). (d) Calibration curves for fenitrothion detection from samples diluted in buffer medium (PBST – black curve) and samples collected in the field (tap water – blue curve). Specificity of the assay is not altered. Adapted from (Ramirez-Priego et al., 2021).

devices. BiMWs encompasses the benefits from evanescent-wave sensors and interferometric configurations in a single-channel structure that addresses the requirements of miniaturization and integration of LOC portable devices. Overall, they pave the road towards the realization of new generation bio-recognition tools that will have a profound impact in several applications such as health-care diagnostics, environmental pollution identification or food quality control.

Declaration of Competing Interest

The authors declare that they have no known competing financial interests or personal relationships that could have appeared to influence the work reported in this paper.

Acknowledgements

LTM and JGR acknowledge the support from the Spanish MCIN/AEI/10.13039/501100011033 through the PID2019-106965RB-C21 project and by the European Union through the operational program of the European Regional Development Fund (FEDER) of the Valencia Regional Government 2014-2020. BDL, MS, and LML acknowledge support of FLAG-ERA grant LEGOCHIP, funded by the Spanish Research Agency (AEI, Ref. PCI2019-111890-2), and financial support from EROICA project (Spanish Ministry of Science and Innovation MCIN, Ref. PID2019-105132RB-I00). The ICN2 is funded by the CERCA program/Generalitat de Catalunya and supported by the Severo Ochoa Centers of Excellence program, funded by the Spanish Research Agency (AEI, grant SEV-2017-0706).

References

Aćimović, S.S., Ortega, M.A., Sanz, V., Berthelot, J., Garcia-Cordero, J.L., Renger, J., Maerkl, S.J., Kreuzer, M.P., Quidant, R., 2014. LSPR chip for parallel, rapid, and sensitive detection of cancer markers in serum. Nano Lett. 14, 2636–2641. https://doi.org/10.1021/nl500574n.

Aikio, S., Hiltunen, M., Hiltunen, J., 2015. Compensation of drift by using a multichannel integrated Young interferometer. Appl. Opt. 54, 4771. https://doi.org/10.1364/AO.54.004771.

Baba, T., 2008. Slow light in photonic crystals. Nat. Photonics 2, 465–473. https://doi.org/10.1038/nphoton.2008.146.

Barrios, C.A., Bañuls, M.J., González-Pedro, V., Gylfason, K.B., Sánchez, B., Griol, A., Maquieira, A., Sohlström, H., Holgado, M., Casquel, R., 2008. Label-free optical biosensing with slot-waveguides. Opt. Lett. 33, 708. https://doi.org/10.1364/OL.33.000708.

Bassols-Cornudella, B., Ramirez-Priego, P., Soler, M., Estevez, M.C., Luis-Ravelo, H.J.D., Cardenosa-Rubio, M., Lechuga, L.M., 2022. Novel sensing algorithm for linear read-out of bimodal waveguide interferometric biosensors. J. Lightwave Technol. 40, 237–244. https://doi.org/10.1109/JLT.2021.3118103.

Bogaerts, W., Pérez, D., Capmany, J., Miller, D.A.B., Poon, J., Englund, D., Morichetti, F., Melloni, A., 2020. Programmable photonic circuits. Nature 586, 207–216. https://doi.org/10.1038/s41586-020-2764-0.

Brimont, A., Thomson, D.J., Sanchis, P., et al., 2011. High speed silicon electro-optical modulators enhanced via slow light propagation. Opt. Express 19, 20876. https://doi.org/10.1364/OE.19.020876.

Bruck, R., Hainberger, R., 2014. Sensitivity and design of grating-assisted bimodal interferometers for integrated optical biosensing. Opt. Express 22, 32344. https://doi.org/10.1364/oe.22.032344.

Cai, H., Parks, J.W., Wall, T.A., Stott, M.A., Stambaugh, A., Alfson, K., Griffiths, A., Mathies, R.A., Carrion, R., Patterson, J.L., Hawkins, A.R., Schmidt, H., 2015. Optofluidic analysis system for amplification-free, direct detection of Ebola infection. Sci. Rep. 5, 14494. https://doi.org/10.1038/srep14494.

Castelló, J.G., V. Toccafondo, J. Escorihuela, M.J. Bañuls, A. Maquieira, J. García-Rupérez, 2012. Real-time analysis of antigen-antibody association kinetics using a low-cost SOI photonic biosensor, IEEE International Conference on Group IV Photonics GFP. 297–299. 10.1109/GROUP4.2012.6324165.

Ceyssens, F., Witters, D., Van Grimbergen, T., Knez, K., Lammertyn, J., Puers, R., 2013. Integrating optical waveguides in electrowetting-on-dielectric digital microfluidic chips. Sensors Actuators, B Chem. 181, 166–171. https://doi.org/10.1016/j.snb.2013.01.078.

Cheben, P., Halir, R., Schmid, J.H., Atwater, H.A., Smith, D.R., 2018. Subwavelength integrated photonics. Nature 560, 565–572. https://doi.org/10.1038/s41586-018-0421-7.

Chocarro-Ruiz, B., Pérez-Carvajal, J., Avci, C., Calvo-Lozano, O., Alonso, M.I., Maspoch, D., Lechuga, L.M., 2018. A CO2 optical sensor based on self-assembled metal-organic framework nanoparticles. J. Mater. Chem. A 6, 13171–13177. https://doi.org/10.1039/c8ta02767f.

Chow, E., Grot, A., Mirkarimi, L.W., Sigalas, M., Girolami, G., 2004. Ultracompact biochemical sensor built with two-dimensional photonic crystal microcavity. Opt Lett. 29, 1093–1095. https://doi.org/10.1364/ol.29.001093.

Chrostowski, L., S. Grist, J. Flueckiger, W. Shi, X. Wang, E. Ouellet, H. Yun, M. Webb, B. Nie, Z. Liang, K.C. Cheung, S.A. Schmidt, D.M. Ratner, N.A.F. Jaeger, 2012. Silicon photonic resonator sensors and devices, Laser Resonators, Microresonators, and Beam Control XIV, SPIE. 823620. 10.14288/1.0107567.

Dante, S., 2014. All-optical phase modulation for advanced interferometric point-of-care biosensors. UAB http://hdl.handle.net/10803/285191.

Dante, S., Duval, D., Fariña, D., González-Guerrero, A.B., Lechuga, L.M., 2015. Linear readout of integrated interferometric biosensors using a periodic wavelength modulation. Laser Photonics Rev. 9, 248–255. https://doi.org/10.1002/lpor.201400216.

De Vos, K., Bartolozzi, I., Schacht, E., Bienstman, P., Baets, R., 2007. Silicon-on-Insulator microring resonator for sensitive and label-free biosensing. Opt. Express 15, 7610. https://doi.org/10.1364/oe.15.007610.

Duval, D., González-Guerrero, A.B., Dante, S., Osmond, J., Monge, R., Fernández, L.J., Zinoviev, K.E., Domínguez, C., Lechuga, L.M., 2012. Nanophotonic lab-on-a-chip platforms including novel bimodal interferometers, microfluidics and grating couplers. Lab Chip 12, 1987–1994. https://doi.org/10.1039/c2lc40054e.

Estevez, M.C., Alvarez, M., Lechuga, L.M., 2012. Integrated optical devices for lab-on-a-chip biosensing applications. Laser Photonics Rev. 6, 463–487. https://doi.org/10.1002/lpor.201100025.

Fernández Gavela, A., Grajales García, D., Ramirez, J., Lechuga, L., 2016. Last advances in silicon-based optical biosensors. Sensors 16, 285. https://doi.org/10.3390/s16030285.

Flueckiger, J., Schmidt, S., Donzella, V., Sherwali, A., Ratner, D.M., Chrostowski, L., Cheung, K.C., 2016. Sub-wavelength grating for enhanced ring resonator biosensor. Opt. Express 24, 15672. https://doi.org/10.1364/oe.24.015672.

Freitag, S., Le Trong, I., Chilkoti, A., Klumb, L.A., Stayton, P.S., Stenkamp, R.E., 1998. Structural studies of binding site tryptophan mutants in the high-affinity streptavidin-biotin complex. J. Mol. Biol. 279, 211–221. https://doi.org/10.1006/jmbi.1998.1735.

Gao, Y., Gan, Q., Xin, Z., Cheng, X., Bartoli, F.J., 2011. Plasmonic Mach-Zehnder interferometer for ultrasensitive on-chip biosensing. ACS Nano 5, 9836–9844. https://doi.org/10.1021/nn2034204.

García-Rupérez, J., L. Torrijos-Morán, 2021. Bimodal Interferometric Photonic Sensors Based On Periodic Configurations, in: OSA Optical Sensors and Sensing Congress, OSA, Washington, D.C., 10.1364/SENSORS.2021.SF2D.1.

García-Ruperez, J., L. Torrijos-Morán, M. Gomez-Gomez, P. Martinez-Perez, S. Ponce-Alcantara, 2021. High performance photonic biosensors based on periodic configurations, in: S.M. García-Blanco, P. Cheben (Eds.), Integrated Optics: Devices, Materials, and Technologies XXV, SPIE, 10.1117/12.2576401.

Giraud, L., Nadarajah, R., Matar, Y., Bazin, G., Sun, J., Zhu, X.X., Giasson, S., 2016. Amino-functionalized monolayers covalently grafted to silica-based substrates as a robust primer anchorage in aqueous media. Appl. Surf. Sci. 370, 476–485. https://doi.org/10.1016/j.apsusc.2016.02.141.

González-Guerrero, A.B., Alvarez, M., Castaño, A.G., Domínguez, C., Lechuga, L.M., 2013. A comparative study of in-flow and micro-patterning biofunctionalization protocols for nanophotonic silicon-based biosensors. J. Colloid Interface Sci. 393, 402–410. https://doi.org/10.1016/j.jcis.2012.10.040.

González-Guerrero, A.B., Maldonado, J., Herranz, S., Lechuga, L.M., 2016. Trends in photonic lab-on-chip interferometric biosensors for point-of-care diagnostics. Anal. Methods 8, 8380–8394. https://doi.org/10.1039/c6ay02972h.

González-Guerrero, A.B., Maldonado, J., Dante, S., Grajales, D., Lechuga, L.M., 2017. Direct and label-free detection of the human growth hormone in urine by an ultrasensitive bimodal waveguide biosensor. J. Biophotonics 10, 61–67. https://doi.org/10.1002/jbio.201600154.

Grajales, D., Fernández Gavela, A., Domínguez, C., Sendra, J.R., Lechuga, L.M., 2019. Low-cost vertical taper for highly efficient light in-coupling in bimodal nanointerferometric waveguide biosensors. J. Phys.: Photonics 1, 025002. https://doi.org/10.1088/2515-7647/aafebb.

Gunnar, B., Carl-Fredrik, M., 2011. Orientation and capturing of antibody affinity ligands: applications to surface plasmon resonance biochips. Sens. Actuators, B 158, 265–270. https://doi.org/10.1016/j.snb.2011.06.017.

Guo, Y., Guo, Y., Li, C., Zhang, H., Zhou, X., Zhang, L., 2021. Integrated optical phased arrays for beam forming and steering. Appl. Sci. 11, 4017. https://doi.org/10.3390/app11094017.

Halir, R., Cheben, P., Luque-González, J.M., Sarmiento-Merenguel, J.D., Schmid, J.H., Wangüemert-Pérez, G., Xu, D.X., Wang, S., Ortega-Moñux, A., Molina-Fernández, Í., 2016. Ultra-broadband nanophotonic beamsplitter using an anisotropic sub-wavelength metamaterial. Laser Photonics Rev. 10, 1039–1046. https://doi.org/10.1002/lpor.201600213.

Heideman, R.G., Lambeck, P.V., 1999. Remote opto-chemical sensing with extreme sensitivity: design, fabrication and performance of a pigtailed integrated optical phase-modulated Mach-Zehnder interferometer system. Sens. Actuators, B 61, 100–127. https://doi.org/10.1016/S0925-4005(99)00283-X.

Heideman, R.G., Kooyman, R.P.H., Greve, J., 1991. Development of an optical waveguide interferometric immunosensor. Sens. Actuators, B 4, 297–299. https://doi.org/10.1016/0925-4005(91)80126-5.

Herranz, S., Gavela, A.F., Lechuga, L.M., 2017. Label-free biosensors based on bimodal waveguide (BiMW) interferometers. Methods Mol. Biol. 1571, 161–185. https://doi.org/10.1007/978-1-4939-6848-0_11.

Hess, D., Yang, T., Stavrakis, S., 2020. Droplet-based optofluidic systems for measuring enzyme kinetics. Anal. Bioanal. Chem. 412, 3265–3283. https://doi.org/10.1007/s00216-019-02294-z.

Huang, C.S., Chaudhery, V., Pokhriyal, A., George, S., Polans, J., Lu, M., Tan, R., Zangar, R.C., Cunningham, B.T., 2012. Multiplexed cancer biomarker detection using quartz-based photonic crystal surfaces. Anal. Chem. 84, 1126–1133. https://doi.org/10.1021/ac202817q.

Huertas, C.S., Fariña, D., Lechuga, L.M., 2016. Direct and label-free quantification of micro-RNA-181a at attomolar level in complex media using a nanophotonic biosensor. ACS Sensors 1, 748–756. https://doi.org/10.1021/acssensors.6b00162.

Irace, A., Breglio, G., Alvarez-Herrero, A., Guerrero, H., Belenguer, T., Levy, D., Rao, Y., Kalli, K., Brady, G., Webb, D., Jackson, D., Zhang, L., 2003. All-silicon optical temperature sensor based on Multi-Mode Interference. Opt. Express 11, 2807–2812. https://doi.org/10.1364/OE.11.002807.

Joannopoulos, J.D., Villeneuve, P.R., Fan, S., 1997. Photonic crystals: putting a new twist on light. Nature 386, 143–149. https://doi.org/10.1038/386143a0.

Krauss, T.F., 2007. Slow light in photonic crystal waveguides. J. Phys. D Appl. Phys. 40, 2666–2670. https://doi.org/10.1088/0022-3727/40/9/S07.

Ksendzov, A., Lin, Y., 2005. Integrated optics ring-resonator sensors for protein detection. Opt. Lett. 30, 3344. https://doi.org/10.1364/OL.30.003344.

Lenz, K.D., Jakhar, S., Chen, J.W., Anderson, A.S., Purcell, D.C., Ishak, M.O., Harris, J.F., Akhadov, L.E., Kubicek-Sutherland, J.Z., Nath, P., Mukundan, H., 2021. A centrifugal microfluidic cross-flow filtration platform to separate serum from whole blood for the detection of amphiphilic biomarkers. Sci. Rep. 11, 5287. https://doi.org/10.1038/s41598-021-84353-z.

Levy, R., Ruschin, S., 2008. Critical sensitivity in hetero-modal interferometric sensor using spectral interrogation. Opt. Express 16, 20516. https://doi.org/10.1364/OE.16.020516.

Levy, R., Ruschin, S., 2009. Design of a single-channel modal interferometer waveguide sensor. IEEE Sens. J. 9, 146–153. https://doi.org/10.1109/JSEN.2008.2011075.

Levy, R., Ruschin, S., Goldring, D., 2009. Critical sensitivity effect in an interferometer sensor. Opt. Lett. 34, 3023. https://doi.org/10.1364/OL.34.003023.

Liang, Y., Zhao, M., Wu, Z., Morthier, G., 2018. Investigation of grating-assisted trimodal interferometer biosensors based on a polymer platform. Sensors. 18, 1502. https://doi.org/10.3390/s18051502.

Liang, Y., Zhao, M., Wu, Z., Morthier, G., 2019. Bimodal waveguide interferometer RI sensor fabricated on low-cost polymer platform. IEEE Photonics J. 11, 1–8. https://doi.org/10.1109/JPHOT.2019.2900741.

Ligler, F.S., 2009. Perspective on optical biosensors and integrated sensor systems. Anal. Chem. 81, 519–526. https://doi.org/10.1021/ac8016289.

Liu, Q., Tu, X., Kim, K.W., Kee, J.S., Shin, Y., Han, K., Yoon, Y.J., Lo, G.Q., Park, M.K., 2013. Highly sensitive Mach-Zehnder interferometer biosensor based on silicon nitride slot waveguide. Sens. Actuators, B 188, 681–688. https://doi.org/10.1016/J.SNB.2013.07.053.

Liu, Q., Kim, K.W., Gu, Z., Kee, J.S., Park, M.K., 2014. Single-channel Mach-Zehnder interferometric biochemical sensor based on two-lateral-mode spiral waveguide. Opt. Express 22, 27910. https://doi.org/10.1364/oe.22.027910.

Lohmeyer, M., Wilkens, L., Zhuromskyy, O., Dotsch, H., Hertel, P., 2001. Integrated magnetooptic cross strip isolator. Opt. Commun. 189, 251–259. https://doi.org/10.1016/S0030-4018(01)01010-0.

Lopez, G.A., Estevez, M.C., Soler, M., Lechuga, L.M., 2017. Recent advances in nanoplasmonic biosensors: applications and lab-on-a-chip integration. Nanophotonics. 6, 123–136. https://doi.org/10.1515/nanoph-2016-0101.

Luan, E., Shoman, H., Ratner, D., Cheung, K., Chrostowski, L., 2018. Silicon photonic biosensors using label-free detection. Sensors. 18, 3519. https://doi.org/10.3390/s18103519.

Luan, E., Yun, H., Ma, M., Ratner, D.M., Cheung, K.C., Chrostowski, L., 2019. Label-free biosensing with a multi-box sub-wavelength phase-shifted Bragg grating waveguide. Biomed. Opt. Express 10, 4825. https://doi.org/10.1364/boe.10.004825.

Luchansky, M.S., Bailey, R.C., 2012. High-Q optical sensors for chemical and biological analysis. Anal. Chem. 84, 793–821. https://doi.org/10.1021/ac2029024.

Maldonado, J., González-Guerrero, A.B., Domínguez, C., Lechuga, L.M., 2016. Label-free bimodal waveguide immunosensor for rapid diagnosis of bacterial infections in cirrhotic patients. Biosens. Bioelectron. 85, 310–316. https://doi.org/10.1016/j.bios.2016.04.095.

Maldonado, J., González-Guerrero, A.B., Fernández-Gavela, A., González-López, J.J., Lechuga, L.M., 2020. Ultrasensitive label-free detection of unamplified multidrug-resistance bacteria genes with a bimodal waveguide interferometric biosensor. Diagnostics 10, 845. https://doi.org/10.3390/diagnostics10100845.

Maldonado, J., Estévez, M.-C., Fernández-Gavela, A., González-López, J.J., González-Guerrero, A.B., Lechuga, L.M., 2020. Label-free detection of nosocomial bacteria using a nanophotonic interferometric biosensor. Analyst 145, 497–506. https://doi.org/10.1039/C9AN01485C.

McDonagh, C., Burke, C.S., MacCraith, B.D., 2008. Optical chemical sensors. Chem. Rev. 108, 400–422. https://doi.org/10.1021/cr068102g.

Miller, D.A.B., 2013. Self-aligning universal beam coupler. Opt. Express 21, 6360. https://doi.org/10.1364/oe.21.006360.

Modi, A., Koratkar, N., Lass, E., Wei, B., Ajayan, P.M., 2003. Miniaturized gas ionization sensors using carbon nanotubes. Nature 424, 171–174. https://doi.org/10.1038/nature01777.

Moon, J.H., Shin, J.W., Kim, S.Y., Park, J.W., 1996. Formation of uniform aminosilane thin layers: An imine formation to measure relative surface density of the amine group. Langmuir 12, 4621–4624. https://doi.org/10.1021/la9604339.

Morichetti, F., Grillanda, S., Carminati, M., Ferrari, G., Sampietro, M., Strain, M.J., Sorel, M., Melloni, A., 2014. Non-invasive on-chip light observation by contactless waveguide conductivity monitoring. IEEE J. Sel. Top. Quantum Electron. 20, 292–301. https://doi.org/10.1109/JSTQE.2014.2300046.

Muñoz, P., Micó, G., Bru, L.A., Pastor, D., Pérez, D., Doménech, J.D., Fernández, J., Baños, R., Gargallo, B., Alemany, R., Sánchez, A.M., Cirera, J.M., Mas, R., Domínguez, C., 2017. Silicon nitride photonic integration platforms for visible, near-infrared and mid-infrared applications. Sensors 17, 2088. https://doi.org/10.3390/S17092088.

Nguyen, H.C., Hashimoto, S., Shinkawa, M., Baba, T., 2012. Compact and fast photonic crystal silicon optical modulators. Opt. Express 20, 22465. https://doi.org/10.1364/OE.20.022465.

Lambeck, P.V., 1992. Integrated opto-chemical sensors. Sens. Actuators, B 8, 103–116. https://doi.org/10.1016/0925-4005(92)85016-P.

Lambeck, P.V., 2006. Integrated optical sensors for the chemical domain. Meas. Sci. Technol. 17, R93–R116. https://doi.org/10.1088/0957-0233/17/8/R01.

Paniccia, M., 2010. Integrating silicon photonics. Nat. Photonics 4, 498–499. https://doi.org/10.1038/nphoton.2010.189.

Parks, J.W., Olson, M.A., Kim, J., Ozcelik, D., Cai, H., Carrion, R., Patterson, J.L., Mathies, R.A., Hawkins, A.R., Schmidt, H., 2014. Integration of programmable microfluidics and on-chip fluorescence detection for biosensing applications. Biomicrofluidics. 8, 054111 https://doi.org/10.1063/1.4897226.

Pérez-Armenta, C., Ortega-Moñux, A., Čtyroký, J., Cheben, P., Schmid, J.H., Halir, R., Molina-Fernández, Í., Wangüemert-Pérez, J.G., 2020. Narrowband Bragg filters based on subwavelength grating waveguides for silicon photonic sensing. Opt. Express 28, 37971. https://doi.org/10.1364/oe.404364.

Prieto, F., Sepúlveda, B., Calle, A., Llobera, A., Domínguez, C., Abad, A., Montoya, A., Lechuga, L.M., 2003. An integrated optical interferometric nanodevice based on silicon technology for biosensor applications. Nanotechnology. 14, 907–912. https://doi.org/10.1088/0957-4484/14/8/312.

Ramirez, J.C., Lechuga, L.M., Gabrielli, L.H., Hernandez-Figueroa, H.E., 2015. Study of a low-cost trimodal polymer waveguide for interferometric optical biosensors. Opt. Express 23, 11985. https://doi.org/10.1364/oe.23.011985.

Ramirez, J.C., Gabrielli, L.H., Lechuga, L.M., Hernandez-Figueroa, H.E., 2019. Trimodal waveguide demonstration and its implementation as a high order mode interferometer for sensing application. Sensors 19, 2821. https://doi.org/10.3390/s19122821.

Ramirez-Priego, P., Estévez, M.-C., Díaz-Luisravelo, H.J., Manclús, J.J., Montoya, Á., Lechuga, L.M., 2021. Real-time monitoring of fenitrothion in water samples using a silicon nanophotonic biosensor. Anal. Chim. Acta 1152, 338276. https://doi.org/10.1016/j.aca.2021.338276.

Ruiz-Vega, G., Soler, M., Lechuga, L.M., 2021. Nanophotonic biosensors for point-of-care COVID-19 diagnostics and coronavirus surveillance. J. Phys.: Photonics 3, 011002. https://doi.org/10.1088/2515-7647/abd4ee.

Sabek, J., Torrijos-Morán, L., Griol, A., Díaz Betancor, Z., Bañuls Polo, M.-J., Maquieira, Á., García-Rupérez, J., 2018. Real time monitoring of a UV light-assisted biofunctionalization protocol using a nanophotonic biosensor. Biosensors 9, 6. https://doi.org/10.3390/bios9010006.

Sabek, J., Díaz-Fernández, F.J., Torrijos-Morán, L., Díaz-Betancor, Z., Maquieira, Á., Bañuls, M.-J., Pinilla-Cienfuegos, E., García-Rupérez, J., 2019. Experimental study of an evanescent-field biosensor based on 1D photonic bandgap structures, Beilstein. J. Nanotechnol. 10, 967–974. https://doi.org/10.3762/bjnano.10.97.

Schipper, E.F., Brugman, A.M., Dominguez, C., Lechuga, L.M., Kooyman, R.P.H., Greve, J., 1997. The realization of an integrated Mach-Zehnder waveguide immunosensor in silicon technology. Sens. Actuators, B 40, 147–153. https://doi.org/10.1016/S0925-4005(97)80254-7.

Schmitt, K., Schirmer, B., Hoffmann, C., Brandenburg, A., Meyrueis, P., 2007. Interferometric biosensor based on planar optical waveguide sensor chips for label-free detection of surface bound bioreactions. Biosens. Bioelectron. 22, 2591–2597. https://doi.org/10.1016/j.bios.2006.10.016.

Schudel, B.R., Choi, C.J., Cunningham, B.T., Kenis, P.J.A., 2009. Microfluidic chip for combinatorial mixing and screening of assays. Lab Chip 9, 1676–1680. https://doi.org/10.1039/b901999e.

Sepúlveda, B., Sánchez Del Río, J., Moreno, M., Blanco, F.J., Mayora, K., Domínguez, C., Lechuga, L.M., 2006. Optical biosensor microsystems based on the integration of highly sensitive Mach-Zehnder interferometer devices. J. Opt. A: Pure Appl. Opt. 8 https://doi.org/10.1088/1464-4258/8/7/S41.

Shimizu, T., Hatori, N., Okano, M., Ishizaka, M., Urino, Y., Yamamoto, T., Mori, M., Nakamura, T., Arakawa, Y., 2014. Multichannel and high-density hybrid integrated light source with a laser diode array on a silicon optical waveguide platform for interchip optical interconnection. Photonics Res. 2, A19. https://doi.org/10.1364/prj.2.000a19.

Soler, M., Lechuga, L.M., 2022. Biochemistry strategies for label-free optical sensor biofunctionalization: advances towards real applicability. Anal. Bioanal. Chem. 414, 5071–5085. https://doi.org/10.1007/s00216-021-03751-4.

Soler, M., Huertas, C.S., Lechuga, L.M., 2019. Label-free plasmonic biosensors for point-of-care diagnostics: a review. Exp. Rev. Mol. Diagnostics 19, 71–81. https://doi.org/10.1080/14737159.2019.1554435.

Son, G., Han, S., Park, J., Kwon, K., Yu, K., 2018. High-efficiency broadband light coupling between optical fibers and photonic integrated circuits. Nanophotonics 7, 1845–1864. https://doi.org/10.1515/nanoph-2018-0075.

Soref, R., 2006. The past, present, and future of silicon photonics. IEEE J. Sel. Top. Quantum Electron. 12, 1678–1687. https://doi.org/10.1109/JSTQE.2006.883151.

Szydzik, C., Gavela, A.F., Herranz, S., Roccisano, J., Knoerzer, M., Thurgood, P., Khoshmanesh, K., Mitchell, A., Lechuga, L.M., 2017. An automated optofluidic biosensor platform combining interferometric sensors and injection moulded microfluidics. Lab Chip 17, 2793–2804. https://doi.org/10.1039/c7lc00524e.

Tao, J., Wang, X., Sun, T., Cai, H., Wang, Y., Lin, T., Fu, D., Ting, L.L.Y., Gu, Y., Zhao, D., 2017. Hybrid photonic cavity with metal-organic framework coatings for the ultra-sensitive detection of volatile organic compounds with high immunity to humidity. Sci. Rep. 7, 41640. https://doi.org/10.1038/srep41640.

Laser Diode Technology, (n.d.). https://www.newport.com/t/laser-diode-technology (accessed April 13, 2022).

Theurer, M., Moehrle, M., Sigmund, A., Velthaus, K.O., Oldenbeuving, R.M., Wevers, L., Postma, F.M., Mateman, R., Schreuder, F., Geskus, D., Worhoff, K., Dekker, R., Heideman, R.G., Schell, M., 2020. Flip-chip integration of InP to SiN photonic integrated circuits. J. Lightwave Technol. 38, 2630–2636. https://doi.org/10.1109/JLT.2020.2972065.

Tien, P.K., 1977. Integrated optics and new wave phenomena in optical waveguides. Rev. Mod. Phys. 49, 361–420. https://doi.org/10.1103/RevModPhys.49.361.

Torrijos-Moran, L., Brimont, A., Griol, A., Sanchis, P., Garcia-Ruperez, J., 2021. Ultra-compact optical switches using slow light bimodal silicon waveguides. J. Lightwave Technol. 39, 3495–3501. https://doi.org/10.1109/JLT.2021.3066479.

Torrijos-Morán, L., A. Griol, J. García-Rupérez, 2020. Bimodal waveguide sensors enabled by subwavelength grating structures, in: OSA Advanced Photonics Congress (AP), OSA, Washington, D.C., 10.1364/IPRSN.2020.ITu4A.4.

Torrijos-Morán, L., García-Rupérez, J., 2019. Single-channel bimodal interferometric sensor using subwavelength structures. Opt. Express 27, 8168. https://doi.org/10.1364/oe.27.008168.

Torrijos-Morán, L., García-Rupérez, J., 2021. Design of slow-light-enhanced bimodal interferometers using dimensionality reduction techniques. Opt. Express 29, 33962. https://doi.org/10.1364/oe.425865.

Torrijos-Morán, L., Griol, A., García-Rupérez, J., 2019. Experimental study of subwavelength grating bimodal waveguides as ultrasensitive interferometric sensors. Opt. Lett. 44, 4702. https://doi.org/10.1364/ol.44.004702.

Torrijos-Morán, L., Martínez-Pérez, P., García-Rupérez, J., 2020. Real-time functionalization and biosensing in subwavelength grating bimodal waveguides. In: 22nd European Conference on Integrated Optics, pp. 1–3.

Torrijos-Morán, L., Griol, A., García-Rupérez, J., 2021. Slow light bimodal interferometry in one-dimensional photonic crystal waveguides. Light Sci. Appl. 10, 16. https://doi.org/10.1038/s41377-020-00460-y.

Uchiyamada, K., Okubo, K., Asakawa, K., Kamon, Y., Kitayama, Y., Takeuchi, T., Suzuki, H., 2019. Perforated bimodal interferometric biosensor for affinity sensing. Adv. Mater. Technol. 4, 1800533. https://doi.org/10.1002/admt.201800533.

Wang, Y., Lu, Z., Ma, M., Yun, H., Zhang, F., Jaeger, N.A.F., Chrostowski, L., 2016. Compact broadband directional couplers using subwavelength gratings. IEEE Photonics J. 8, 1–8. https://doi.org/10.1109/JPHOT.2016.2574335.

Wangüemert-Pérez, J.G., Hadij-ElHouati, A., Sánchez-Postigo, A., Leuermann, J., Xu, D.-X., Cheben, P., Ortega-Moñux, A., Halir, R., Molina-Fernández, Í., 2019. Subwavelength structures for silicon photonics biosensing. Opt. Laser Technol. 109, 437–448. https://doi.org/10.1016/j.optlastec.2018.07.071.

Yavari, F., Chen, Z., Thomas, A.V., Ren, W., Cheng, H.M., Koratkar, N., 2011. High sensitivity gas detection using a macroscopic three-dimensional graphene foam network. Sci. Rep. 1, 166. https://doi.org/10.1038/srep00166.

Yavas, O., Svedendahl, M., Dobosz, P., Sanz, V., Quidant, R., 2017. On-a-chip biosensing based on all-dielectric nanoresonators. Nano Lett. 17, 4421–4426. https://doi.org/10.1021/acs.nanolett.7b01518.

Ymeti, A., Kanger, J.S., Greve, J., Lambeck, P.V., Wijn, R., Heideman, R.G., 2003. Realization of a multichannel integrated Young interferometer chemical sensor. Appl. Opt. 42 (28), 5649.

Zeming, K.K., Thakor, N.V., Zhang, Y., Chen, C.H., 2016. Real-time modulated nanoparticle separation with an ultra-large dynamic range. Lab Chip 16, 75–85. https://doi.org/10.1039/c5lc01051a.

Zhang, F., Sautter, K., Larsen, A.M., Findley, D.A., Davis, R.C., Samha, H., Linford, M.R., 2010. Chemical vapor deposition of three aminosilanes on silicon dioxide: Surface characterization, stability, effects of silane concentration, and cyanine dye adsorption. Langmuir 26, 14648–14654. https://doi.org/10.1021/la102447y.

Zhao, X., Dalir, H., Xu, X., Chen, R.T., 2017. Efficient coupling into slow-light one-dimensional fishbone waveguide by mode converter method. Appl. Phys Express 10, 072502. https://doi.org/10.7567/APEX.10.072502/XML.

Zinoviev, K.E., González-Guerrero, A.B., Domínguez, C., Lechuga, L.M., 2011. Integrated bimodal waveguide interferometric biosensor for label-free analysis. J. Lightwave Technol. 29, 1926–1930. https://doi.org/10.1109/JLT.2011.2150734.